Effects of anisotropy in tridimensional diffusion: flow patterns and transport efficiency

Piyush Awasthi[1], Mahendhar Kumar[2] and Yana Nec[3]
[1] School of Biomedical Engineering, University of British Columbia, British Columbia, Canada
[2] School of Mechanical Engineering, Vellore Institute of Technology, Tamilnadu, India
[3] Department of Mathematics and Statistics, Thompson Rivers University, British Columbia, Canada

Abstract. Modelling diffusive processes via a constant effective diffusivity value taken to represent realistic uncertainty or heterogeneity is entrenched in scientific and engineering applications. This brings forth the question to what extent the flow pattern changes when symmetry is broken by anisotropy. This study supplies the answer by deriving a class of tridimensional solutions to the steady non-linear diffusion equation in a spherical domain divided into an arbitrary number of meridian sectors with distinct diffusivities and generation rates. The new family of solutions permits flexible modelling, where traditionally only isotropic radial transport was considered. The flow patterns support an extensive variety of topological terrain via tesseral and sectoral harmonics. The anisotropy gives rise to an unconventional type of a fixed point combining both node and saddle attributes. The contours are non-smooth on the contiguity planes between sectors and might or might not be localised in the polar angle φ and/or azimuthal angle θ, implying a particle might remain confined to a relatively small neighbourhood or meander over the sphere. The impact on motion trajectories and thus transport efficiency implies the energy required to sustain a steady flow is starkly underestimated when symmetry is assumed for simplicity despite the presence of anisotropy.

Keywords. non-linear diffusion equation, exact solutions, anisotropy, spherical coordinates, sectoral and tesseral harmonics, transport efficiency

AMS subject classifications. 35Q35, 76E30, 76N10, 76S05

1 Background

The non-linear diffusion equation (suitably scaled)

$$\partial_t u + \nabla \cdot \left(-Ku^{\gamma-1}\nabla u\right) = C \tag{1}$$

emerges in numerous applications. The scalar field u induces the vector flux $\left(-Ku^{\gamma-1}\right)\nabla u$ that obeys the conservation law (1) subject to the bulk source C. The non-linearity parameter γ is constant and connected to the physical interpretation of u and its flux, whereas the diffusivity K generally need not be constant. In the problem of diffusion within a semiconductor the function u represents the dopant concentration and the compound $Ku^{\gamma-1}$ models the diffusivity at high concentrations with K taken constant and γ assuming values $\gamma = 2$ for arsenic and boron in silicon, $\gamma = 3$ for phosphorus in silicon and $\gamma = 4$ for zinc in gallium [15, and references therein]. When a thin liquid film spreads under gravity, equation (1) governs the surface shape with $K = 1/3$ and non-linearity $\gamma = 4$ originating from the material derivative during the surface motion [20, 14, 22]. In toroidal fusion plasma devices u stands for the temperature of plasma ions and the non-linearity depends on the operating regime [2]. In thermostatistics u is a particle density function with $\gamma \neq 1$ being a measure of non-extensivity [9]. In porous media flows u might be the concentration of a liquid solvent spreading in a polymer with γ related to material expansion [33] or the pressure of percolating gas [5], where $\gamma = 2$ stems from the fluid compressibility. In radiative heat transfer $\gamma = 7$ [21] and for moisture transport in some soils $\gamma = 8$ [8]. These higher values prompted the construction of the mesa-type limit solution for $\gamma \longrightarrow \infty$ using singular perturbation theory [8]. Fractional as well as negative powers of γ are also possible: for instance, in heat conduction $\gamma = -1/3$ for silicon and $\gamma = 1/3$ for superfluid helium [16, 35, and references therein], diffusion from an instantaneous source has $\gamma = -1$ [equation (3.3) of 18], whilst in radiation in ionised gases $6.5 < \gamma < 7.5$ [8]. The dates on these studies are evidence that the interest in equation (1) has not abated in fifty years. Although many of these applications involve a sustained flow, the predominant solution method is a reduction to an ordinary differential equation via a similarity variable combining powers of time and a single spatial coordinate, inevitably decaying in time [4]. Even when starting initially in $\mathbb{R}^n$, the coordinates are quickly reduced to a new space of one spatial dimension implying radial symmetry, and then the similarity is invoked [19]. Furthermore, such similarity solutions of (1) are not possible where a bulk source is present, for instance in heat transfer with an ongoing exothermic reaction,

in aquifer sparging, where the remediation reaction removes the diffusant compounds, or in natural gas and landfill gas flows through their generating media.

The similarity technique was well established by the mid 1960's [1] and is accepted as classical today. Notwithstanding, distinct solution methods emerge and find service in applications. Adomian decomposition was utilised to derive exact solutions to special cases that are both t and x dependent, but are not of the similarity type [35]. Steady exact solutions available to date are scarce and of little practical use due to limiting assumptions and in particular the inability to satisfy generic boundary conditions, cf. [16, equations (3.20)–(3.23)] and [35, equation (28)]. In n dimensions the radially symmetric case with $\gamma = 1/2$ was solved with unity diffusivity and no source [17]. One-dimensional solutions in polar and spherical geometry do allow for conventional boundary conditions as well as bulk generation or degradation, a result considerably more valuable in practice [36]. Albeit derived for $\gamma = 2$, these are easily extensible to any γ.

The difficulty of attaining exact solutions escalates quickly when the desired setting is made more generic, e.g. arbitrary γ, anisotropic K, inhomogeneous right-hand side, higher spatial dimension etc. As a result, gleaning symmetry properties [7] or rigorous bounds [6] has become an area of research unto itself. One observation unifying all foregoing studies is that the partial differential transport equation is reduced to an ordinary differential equation. For decades the only steady exact solutions obtained that way were limited to the radially symmetric setting with different levels of genericity in the aforementioned attributes. Hence the extensive exploration of the self-similarity class. By contrast, steady state solutions have seen meagre development despite various applications evincing a clear need of an anisotropic framework, since in reality the diffusivity is rarely constant. In large environmental applications such as aquifers, natural gas wells and landfills, a constant effective value is often regarded as the only option due to the highly labile properties of the porous matrix. The spatial heterogeneity due to either intrinsic changes or external influence impedes accurate flow modelling and design of effectively functioning engineering systems. The development of tridimensional matrix penetrating imaging techniques such as gas diffusion nuclear magnetic resonance [24] is a testament to the importance of access to reliable permeability data that eventually are translated into the mathematical diffusivity parameter K. Assumption of constant diffusivity hinders the identification of preferential directions of flow [10, 13], correct delineation of the zone of influence[1] [23, 32] or estimation of source strength [34]. In smaller applications this is no less important, as only a faithful approximation of the diffusivity can lead to a successful delivery of the desired fluid to its target [26]. A groundbreaking class of exact solutions with a sufficiently flexible anisotropy function to accommodate custom practical needs was found in a planar geometry [29]. Whilst planar flow fields furnish useful insight, only a tridimensional flow can be deemed realistic. The current study's aim is to construct solutions in spherical geometry with anisotropy and analyse the resultant transport asymmetry. It will be shown that the presence of anisotropy strongly undermines radial transport. In particular, the introduction of a distinct diffusivity in a small portion of the domain engenders significant global changes in the flow field, transferring kinetic energy to the two angular velocity components and creating numerous nearly stagnant locales. This effect cannot be explained via regular perturbation theory and has a profound impact on the flow field in applications, where anisotropy is neglected.

2 General solution

Spherical coordinates are congruous with situations where fluid dispersion or collection is localised around a central point of interest. As long as such a point can be designated, the physical boundaries of the domain need not be spherical, since the constructed solutions might be extended to any geometry by the correspondence of the Cartesian and spherical coordinates. Therefore consider a spherical domain of external radius $r_{\mathcal{X}}$ and core radius $r_{\mathcal{C}} \geqslant 0$: $\mathfrak{B} = \left\{(r, \varphi, \theta) \,|\, r_{\mathcal{C}} \leqslant r \leqslant r_{\mathcal{X}},\ 0 \leqslant \varphi \leqslant \pi,\ 0 \leqslant \theta < 2\pi\right\}$. Let φ and θ denote the polar (latitude) and azimuthal (longitude) angles respectively, as shown in figure 1. In practice the spherical nature of the problem is sometimes broken by the existence of a tube injecting fluid into or drawing it from the domain centre. As long as the injection / suction site is deep enough and much smaller than the external radius $r_{\mathcal{X}}$, it is possible to use the spherical approximation. Mathematically this might be expressed via the requirement $r_{\mathcal{C}} \ll r_{\mathcal{X}}$. One such example is a vertical well made of a solid wall pipe injecting remediating compounds into a contaminated aquifer or collecting natural gas. The ground naturally comprises heterogeneous regions, such as fractured rock, solid rock, saturated or unsaturated sand, clay, silt

[1] The zone of influence is defined as the region, where the head induced at the well results in fluid transport in the surrounding medium: dispersion of the injected reactive compounds in sparging wells and fluid collection in gas or hydraulic wells.

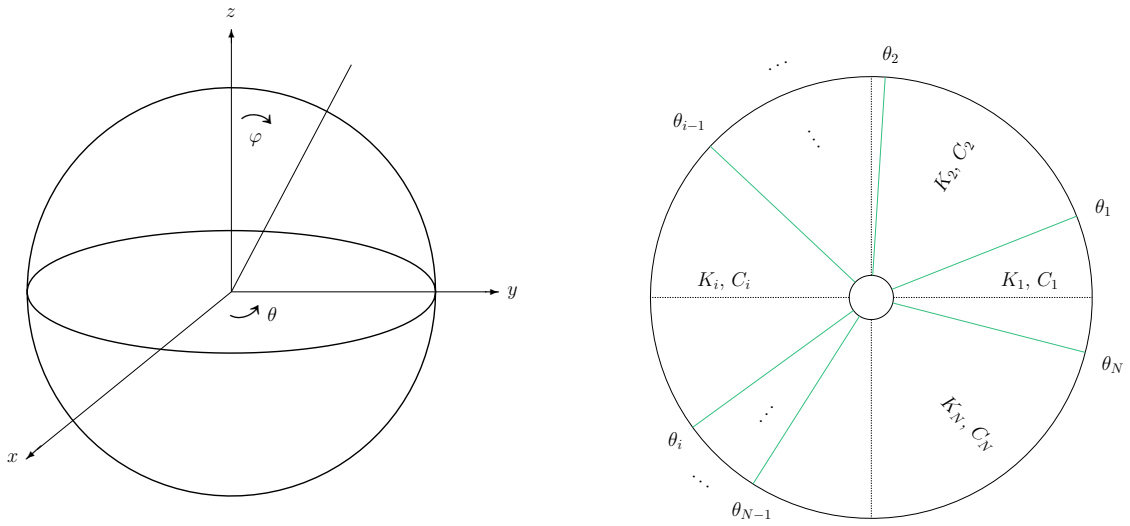

Figure 1: Spherical coordinates notation (left) and division into sectors of distinct diffusivity and/or source strength (equator cross-section, right). Dimensions not to scale.

etc. The diffusivity in these media varies significantly, rendering the assumption of a single effective value for the entire domain untenable. Fractures in particular induce preferential flow directions, i.e. thin wedges where the diffusivity is many orders of magnitude higher than in the surrounding substrate. In landfills the medium consists of compacted waste of many types: demolition and land clearing, household, organic etc. The typical fragment size of the solid matrix and thus the associated diffusivity again range several orders of magnitude. There is no attempt to mix the different types of waste, resulting in distinct porous media. An equivalent example is a needle injecting a solvent into a polymer or a drug into tissue. The polymer's molecular structure naturally induces preferential directions of motion, whereas tissue heterogeneity, e.g. muscle, bone or cartilage at different angles around the needle tip, brings about a situation similar to the landfill media. Another example from the area of biomedicine has been discussed in [30]: injecting certain diffusing compounds into the brain reveals the structure of the extracellular space, which has been likened to foam and is known to offer multiple preferential directions of motion that might be thought of as thin slivers of high diffusivity.

Although the physical dimensions of wells differ starkly from needles, the characteristic length ratio $r_{\mathcal{C}}/r_{\mathcal{X}}$ renders the two frameworks mathematically alike. Aligning the z axis with the well or needle, and setting the origin at the extraction / injection point, in both cases the symmetry is broken along the line $\varphi = 0$. Another example is a horizontal landfill gas well, commonly consisting of a long pipe with equidistant apertures, whose dimensions are extremely small compared to the length of the solid pipe in between, as is the pipe radius [28]. This system's geometry is cylindrical when viewed in its entirety; however, on an intermediate length scale around one set of apertures – far enough from the next closest perforated section, yet not too close to the pipe wall itself – the flow conforms to a spherical geometry. The horizontal well can be thus thought of as a series of sink points controlling spherical flow fields with a progressively diminishing reach as the suction imposed at the well outlet dissipates upstream. Aligning the z axis with the pipe and positioning the origin at the perforated section, the spherical symmetry breaking line is $\varphi = 0$ as well as $\varphi = \pi$. Figure 2 shows the two variants of broken symmetry.

The unknown function u might attain $\mathcal{O}(1)$ values as in the problem of liquid film, where it represents the height of the dispersing fluid; it might be naturally limited to the range $0 \leqslant u \leqslant 1$ as the concentration of a diffusing substance; as the temperature of plasma ions $u \sim \mathcal{O}\left(10^2\right)$, whilst as the absolute pressure of fluid in porous medium flow its values might be on the order of $\mathcal{O}\left(10^5\right)$. It is thus advisable to define the mapping $u \longmapsto u_{\mathcal{X}}\tilde{u}$, where $\tilde{u}$ is a non-dimensional quantity satisfying $0 \leqslant \tilde{u} \leqslant 1$ and $u_{\mathcal{X}}$ is a reference value equal to or exceeding $\max_{\mathfrak{B}} u$. Since the only length coordinate is r, the diffusivity K might be non-dimensionalised

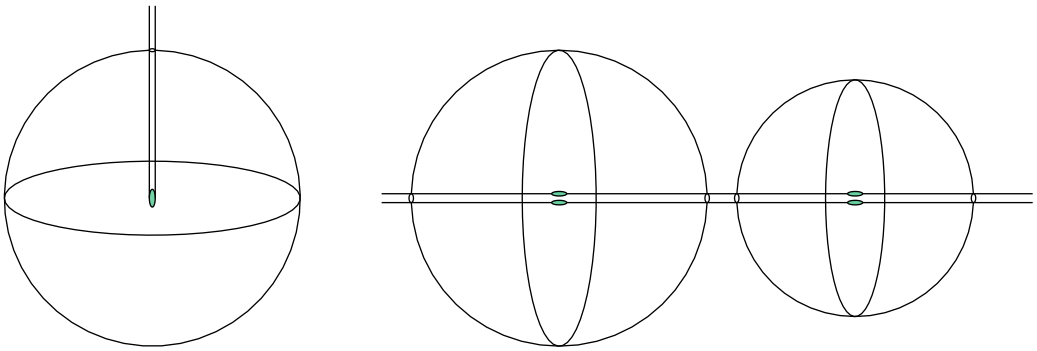

Figure 2: Approximate spherical geometry in applications with symmetry broken along $\varphi = 0$ (single source or sink point, left) and $\varphi = 0, \pi$ (multiple source or sink points, right). Green / grey beads mark injection or extraction sites. Spheres delineate zones of influence rather than physical boundaries. Dimensions not to scale.

by $K \longmapsto r_{\mathcal{X}}^2 \tilde{K}$. The corresponding mapping for the generation rate C is then $C \longmapsto u_{\mathcal{X}}^{\gamma} \tilde{C}$. When either the order of magnitude of $u_{\mathcal{X}}$ or γ is high, the non-dimensional value of C might be very small. Nonetheless, if the physics of the system includes a source or sink, $|C| \ll 1$ should not be neglected based solely on its magnitude. As part of the analysis below it is shown that this decision bears on the solution existence and its degrees of freedom, and thus should be made with caution upon scrutiny of the full solution. Henceforward all quantities are non-dimensional and the tilde symbols are omitted.

Suppose that enough information is available on the variation of diffusivity within the domain in order to divide it into N longitudinal (meridian) sectors that are sufficiently homogeneous to allow an isotropic description therein, as depicted in figure 1. The sectors need not be equal and there is no restriction on their number, as long as no attempt is made to create a smooth variation via the limit $N \longrightarrow \infty$. The general solution is derived in §2. The flow patterns and associated degrees of freedom for two sectors are analysed in §3 and further generalised to an arbitrary number of sectors in §4.

The first step of constructing an exact solution for a multiple sector configuration is to obtain a solution within one isotropic sector. Equation (1) can be written as

$$\Delta u^{\gamma} = -\frac{\gamma C}{K}, \tag{2a}$$

where the subscripts were omitted for simplicity and the Laplacian of a scalar function $u(r, \varphi, \theta)$ in spherical coordinates is given by

$$\Delta u = \frac{1}{r^2} \frac{\partial}{\partial r}\left(r^2 \frac{\partial u}{\partial r} \right) + \frac{1}{r^2 \sin\varphi} \frac{\partial}{\partial \varphi}\left(\sin\varphi \frac{\partial u}{\partial \varphi} \right) + \frac{1}{r^2 \sin^2\varphi} \frac{\partial^2 u}{\partial \theta^2} \,. \tag{2b}$$

Seeking a separation of variables solution and balancing the inhomogeneity in equation (2a) via a purely radial function yields

$$u^{\gamma} = -\frac{\gamma C}{6K} r^2 + \sum_{n=0}^{\infty} \sum_{m=0}^{n} \mathcal{P}_n^m(\cos\varphi) \left\{ r^n \Big(a_{nm} \sin(m\theta) + b_{nm} \cos(m\theta) \Big) + \frac{1}{r^{n+1}} \Big(\alpha_{nm} \sin(m\theta) + \beta_{nm} \cos(m\theta) \Big) \right\}, \tag{3a}$$

where the function $\mathcal{P}_n^m(x)$ is the associated Legendre function of degree n and order m defined as [12, **8.910**]

$$\mathcal{P}_n^m(x) = \frac{(-1)^m}{2^n n!} \left(1 - x^2\right)^{m/2} \frac{\mathrm{d}^{n+m}}{\mathrm{d}x^{n+m}} \left(x^2 - 1\right)^n , \tag{3b}$$

and a_{nm}, b_{nm}, α_{nm} and β_{nm} are constants to be determined. The inhomogeneity term in (3a) implies that the relevant independent compounds are ratios of diffusivities and generation rates rather than the

parameters themselves. As long as $C_i \neq 0 \ \forall \ 1 \leqslant i \leqslant N$, it is possible to define a uniform generation rate C_* and map $K_i \longmapsto K_i C_*/C_i$. Therefore hereinafter the rates C_i are taken equal throughout the domain without loss of generality.

Restricted to any spherical shell of a given radius r_o, the function $u(r_o, \varphi, \theta)$ possesses fixed points at the poles. Differentiation of (3a) with respect to φ will always create a factor $\sin\varphi$ that will vanish at $\varphi = 0$ and $\varphi = \pi$. The derivative with respect to θ vanishes due to different reasons for various combinations of m and n: for all $0 < m \leqslant n$ the associated Legendre functions satisfy $\mathcal{P}_n^m(\pm 1) = 0$, so $\partial_\theta u(r_o, \varphi, \theta) = 0$ at $\varphi = 0, \pi$ regardless of θ, whereas the order $m = 0$ removes the dependence on θ altogether for any n. The type of these two universally present fixed points cannot be unambiguously determined. Whilst for two sector configurations numerical evidence suggests they might be either saddles or nodes, for $N > 2$ they defy conventional classification. Because the poles belong to *all* contiguity planes between sectors of distinct diffusivities, the contour shape nearby might be in keeping with a classical saddle point in some sectors (open paths approaching and then moving away), but characteristic of a node in others (trajectories that would have been closed had that sector's solution been extended to the full span of the azimuthal angle θ). If the point is of the same type in all sectors, it is to be referred to as node or saddle as required. Notwithstanding, the trajectories in its vicinity, whilst generally of a shape reminiscent of the expected in classical settings, including the stable or unstable nature thereof, have an uncommon overall appearance. For nodes the prominent attribute is points of non-smoothness. Saddles feature more than two characteristic directions as well as possible closing of incoming and outgoing trajectories into closed contours. If the point type varies between sectors, it is of a mixed type and might exhibit blended properties. The same classification equally applies to such points formed on boundaries between sectors away from the poles. Examples of these situations are given below when the topology of the flow field u is explored.

The single sector solutions (3a) with distinct values of K_i as well as constants $a_{nm}^{(i)}$, $b_{nm}^{(i)}$, $\alpha_{nm}^{(i)}$ and $\beta_{nm}^{(i)}$, form a sequence $\{u_i\}_{i=1}^N$ that upon satisfying certain continuity requirements on the contiguity planes comprises the solution u in the entire domain $\mathfrak{B}$. The sought function u must be differentiable at least twice within each isotropic subdomain with respect to all coordinates to satisfy (2a), but this level of smoothness is not required on the semi-annuli $\Big\{(r, \varphi, \theta) \,|\, r_{\mathcal{C}} \leqslant r \leqslant r_{\mathcal{X}},\ 0 \leqslant \varphi \leqslant \pi,\ \theta = \theta_i\Big\}$. Since u is a physical quantity such as concentration, temperature or pressure, it must be continuous throughout and in particular on these contiguity planes. Thus

$$u_i(r, \varphi, \theta_i) = u_{i+1}(r, \varphi, \theta_i), \quad 1 \leqslant i \leqslant N, \tag{4a}$$

with $u_{N+1} := u_1$ creating the periodicity necessitated by the spherical geometry. The divergence form of the governing equation (1) implies that the compound $-Ku^{\gamma-1}\nabla u$ represents flux and is the quantity of interest to be conserved. Consider an infinitesimally small horizontal arc straddling the contiguity surface $\theta = \theta_i$. Upon integration of both sides of (1) along this arc and observation that by continuity of u the components in directions r and φ vanish, one arrives at

$$K_i \frac{\partial u_i}{\partial \theta}\bigg|_{(r,\varphi,\theta_i)} = K_{i+1} \frac{\partial u_{i+1}}{\partial \theta}\bigg|_{(r,\varphi,\theta_i)}, \quad 1 \leqslant i \leqslant N, \tag{4b}$$

where defining $K_{N+1} := K_1$ creates the generalisation for the last contiguity plane. Conditions (4) are not enforceable for certain combinations of diffusivities K_i and angles θ_i. In such a case (1) possesses no steady state solution. Construction of exact solutions permits to predict such occurrences. The complete analysis of these singularities is given in §4.1.

3 Two sectors

The simplest family of solutions is constructed for a configuration of two sectors with diffusivities K_1 and K_2. The governing equation is rotationally invariant in θ, allowing to set the contiguity planes as $\theta_1 = \theta_o$ and $\theta_2 = \pi - \theta_o$ with $-\pi/2 < \theta_o < \pi/2$.

3.1 Flow patterns for $n \leqslant 2$

Solutions with a small number of harmonics are instructive since their characteristics are more readily discerned. Juxtaposition of the functional forms of the generation term and homogeneous part in (3a) allows

to infer that the double sum must not be truncated before $n = 2$. Definition (3b) in conjunction with trigonometric identities for $n \leqslant 2$ yields

$$u_i^\gamma = -\frac{\gamma C}{6K_i}\, r^2 + b_{00}^{(i)} + \frac{\beta_{00}^{(i)}}{r} + \cos\varphi \left\{ r b_{10}^{(i)} + \frac{\beta_{10}^{(i)}}{r^2} \right\} - \sin\varphi \left\{ r\left(a_{11}^{(i)} \sin\theta + b_{11}^{(i)} \cos\theta \right) + \frac{1}{r^2}\left(\alpha_{11}^{(i)} \sin\theta + \beta_{11}^{(i)} \cos\theta \right) \right\} +$$

$$\frac{3}{2}\left(\frac{1}{2}\cos(2\varphi) + \frac{1}{6} \right) \left\{ r^2 b_{20}^{(i)} + \frac{\beta_{20}^{(i)}}{r^3} \right\} - \frac{3}{2}\sin(2\varphi) \left\{ r^2\left(a_{21}^{(i)} \sin\theta + b_{21}^{(i)} \cos\theta \right) + \frac{1}{r^3}\left(\alpha_{21}^{(i)} \sin\theta + \beta_{21}^{(i)} \cos\theta \right) \right\} +$$

$$\frac{3}{2}\Big(1 - \cos(2\varphi) \Big) \left\{ r^2\left(a_{22}^{(i)} \sin(2\theta) + b_{22}^{(i)} \cos(2\theta) \right) + \frac{1}{r^3}\left(\alpha_{22}^{(i)} \sin(2\theta) + \beta_{22}^{(i)} \cos(2\theta) \right) \right\}. \tag{5}$$

Conditions (4) on $\theta = \theta_o$ and $\theta = \pi - \theta_o$ must hold for all r and φ, inducing a separation of the coefficients in (5) into groups based on the respective functional forms. Imposing (4a) for the only constant term yields $b_{00}^{(1)} = b_{00}^{(2)}$, which allows to define $b_{00} := b_{00}^{(i)}$, i={1,2}. Henceforth coefficient notation with the superscript omitted is used whensoever coefficients are equal in all sectors. Equation (4b) is satisfied unconditionally. Similar arguments lead to $\beta_{00} := \beta_{00}^{(i)}$, $b_{10} := b_{10}^{(i)}$ and $\beta_{10} := \beta_{10}^{(i)}$. For the coefficients of $r\sin\varphi$ conditions (4) give the system

$$\left(a_{11}^{(1)} - a_{11}^{(2)} \right) \sin\theta_o = 0, \quad \left(b_{11}^{(1)} - b_{11}^{(2)} \right) \cos\theta_o = 0, \tag{6a}$$

$$\left(K_1 a_{11}^{(1)} - K_2 a_{11}^{(2)} \right) \cos\theta_o = 0, \quad \left(K_1 b_{11}^{(1)} - K_2 b_{11}^{(2)} \right) \sin\theta_o = 0. \tag{6b}$$

Since $\cos\theta_o \neq 0$, $b_{11} := b_{11}^{(i)}$ and $a_{11}^{(2)} = K_2 \big/ K_1 a_{11}^{(1)}$ follow. If $\theta_o \neq 0$, $a_{11}^{(i)} = b_{11}^{(i)} = 0$ must hold. If $\theta_o = 0$, one coefficient out of each pair $a_{11}^{(i)}$ and $b_{11}^{(i)}$ remains a degree of freedom. An identical argument applies to the coefficients $\alpha_{11}^{(i)}$, $\beta_{11}^{(i)}$, $a_{21}^{(i)}$, $b_{21}^{(i)}$, $\alpha_{21}^{(i)}$ and $\beta_{21}^{(i)}$. For the coefficients of r^{-3} conditions (4) upon rearrangement result in

$$\frac{1}{4}\left(\beta_{20}^{(1)} - \beta_{20}^{(2)} \right) + \frac{3}{2}\cos(2\theta_o) \left(\beta_{22}^{(1)} - \beta_{22}^{(2)} \right) = 0, \quad \left(\alpha_{22}^{(1)} - \alpha_{22}^{(2)} \right) \sin(2\theta_o) = 0, \tag{7a}$$

$$\left(K_1 \beta_{22}^{(1)} - K_2 \beta_{22}^{(2)} \right) \sin(2\theta_o) = 0, \quad \left(K_1 \alpha_{22}^{(1)} - K_2 \alpha_{22}^{(2)} \right) \cos(2\theta_o) = 0. \tag{7b}$$

This is not a closed system, and moreover $\theta_o = 0$ or $\theta_o = \pi/4$ might satisfy some of these equations. Out of the concomitant quadruple of equations ensuing for the coefficients of $r^{-3}\cos(2\varphi)$, only one is new:

$$\frac{3}{4}\left(\beta_{20}^{(1)} - \beta_{20}^{(2)} \right) - \frac{3}{2}\cos(2\theta_o) \left(\beta_{22}^{(1)} - \beta_{22}^{(2)} \right) = 0, \tag{7c}$$

completing the linear system. Summing (7c) and the first equality in (7a) gives $\beta_{20} := \beta_{20}^{(i)}$. Formulating (4) for the terms of the type r^2 gives

$$\frac{1}{4}\left(b_{20}^{(1)} - b_{20}^{(2)} \right) + \frac{3}{2}\cos(2\theta_o) \left(b_{22}^{(1)} - b_{22}^{(2)} \right) = \frac{\gamma C}{6}\left(\frac{1}{K_1} - \frac{1}{K_2} \right), \quad \left(a_{22}^{(1)} - a_{22}^{(2)} \right) \sin(2\theta_o) = 0, \tag{8a}$$

$$\left(K_1 b_{22}^{(1)} - K_2 b_{22}^{(2)} \right) \sin(2\theta_o) = 0, \quad \left(K_1 a_{22}^{(1)} - K_2 a_{22}^{(2)} \right) \cos(2\theta_o) = 0. \tag{8b}$$

The corresponding system for the coefficients of $r^2\cos(2\varphi)$ contributes only one independent equation:

$$\frac{3}{4}\left(b_{20}^{(1)} - b_{20}^{(2)} \right) - \frac{3}{2}\cos(2\theta_o) \left(b_{22}^{(1)} - b_{22}^{(2)} \right) = 0. \tag{8c}$$

Combining (8c) with the first equality in (8a) yields

$$b_{20}^{(1)} - b_{20}^{(2)} = \frac{\gamma C}{6}\left(\frac{1}{K_1} - \frac{1}{K_2} \right), \quad \cos(2\theta_o) \left(b_{22}^{(1)} - b_{22}^{(2)} \right) = \frac{\gamma C}{12}\left(\frac{1}{K_1} - \frac{1}{K_2} \right), \tag{9}$$

whereby if a solution is to exist for any non-vanishing generation rate C, $\theta_o \neq \pm\pi/4$. A right-angled sector configuration defined by $\theta_o = \pm\pi/4$ does not possess a solution of the separation of variables type. This is a persistent singularity that has also been noted in planar flow in polar coordinates [29]. For all $\theta_o \neq \pm\pi/4$

$$b_{22}^{(1)} - b_{22}^{(2)} = \frac{\gamma C}{12\cos(2\theta_o)}\left(\frac{1}{K_1} - \frac{1}{K_2}\right). \tag{10}$$

The only distinction remaining is whether $\theta_o = 0$ or $\theta_o \neq 0$. In the latter case (10) and the first equality in (8b) form a system with a unique solution $b_{22}^{(i)} = \gamma C \Big/ \Big(12K_i\cos(2\theta_o)\Big)$, $i = \{1, 2\}$. The first equality in (9) gives the relation between $b_{20}^{(i)}$, and it was already established that $\beta_{20}^{(i)}$ must equal, i.e. one degree of freedom remains for either pair, whilst $\alpha_{22}^{(i)} = \beta_{22}^{(i)} = a_{22}^{(i)} = 0$. If $\theta_o = 0$, the first equality in (8b) is satisfied automatically, leaving one coefficient out of the $b_{22}^{(i)}$ pair a degree of freedom. Similarly $\alpha_{22}^{(i)}, \beta_{22}^{(i)}$ and $a_{22}^{(i)}$ pairs have one degree of freedom each.

To complete the resulting class of flows, boundary conditions must be prescribed in one of the sectors. The second sector's solution will follow by the continuity requirements derived above, including on the boundaries. To implement Dirichlet boundary conditions of values $u_{\mathcal{C}}$ and $u_{\mathcal{X}}$ on the core and external spherical shells $r = r_{\mathcal{C}}$ and $r = r_{\mathcal{X}}$ respectively, focus on the first three terms in solution (5) and the sector delimited by $\theta_o \leqslant \theta \leqslant \pi - \theta_o$:

$$\begin{pmatrix} 1 & 1/r_{\mathcal{C}} \\ 1 & 1/r_{\mathcal{X}} \end{pmatrix}\begin{pmatrix} b_{00} \\ \beta_{00} \end{pmatrix} = \begin{pmatrix} u_{\mathcal{C}}^{\gamma} + \dfrac{\gamma C}{6K_2}\, r_{\mathcal{C}}^2 \\ \\ u_{\mathcal{X}}^{\gamma} + \dfrac{\gamma C}{6K_2}\, r_{\mathcal{X}}^2 \end{pmatrix}. \tag{11}$$

The reason the boundary conditions are limited to the first three terms is twofold. Mathematically two conditions can only determine two coefficients. From the vantage point of physics, these three terms are the most significant ones in magnitude. Evidence thereof is to be given below. System (11) always possesses a unique solution. Note that it is possible to have a full spherical domain with $r_{\mathcal{C}} = 0$ and β_{00} as well as all coefficients of negative powers of r vanishing. Henceforth examples for the generic case of $r_{\mathcal{C}} > 0$ are presented.

The constructed family of solutions has an extensive parameter space and effects a considerable variety of flow patterns that is best illustrated using contours on a spherical shell of a fixed radius r_o. In a radially symmetric flow the function u restricted to such a shell would have been constant and thus incapable of producing closed contours. The mere ability to display a well defined level set demonstrates the emergence of strong tangential flow components. The qualitative properties of the pattern (fixed points, φ and θ gradients, separatrices) are not altered when r_o varies, proving that the tangential flow persists throughout the domain.

Depending on the physical meaning ascribed to the scalar function u, there is a number of vector functions associated with it: gradient ∇u, flux $-Ku^{\gamma-1}\nabla u$ and velocity $-K\nabla u$ (possibly up to a constant in dimensional quantities). All possess at least one discontinuous component and are extremely difficult to visualise effectively, since their norm generally spans several orders of magnitude and thus cannot be represented by proportionate arrow length. The level set comprises continuous contours that provide a consistent depiction of the flow field throughout the parameter space, regardless of whether the main interest lies in u itself or the concomitant vector functions.

In light of the above, projections of u on the $\theta - \varphi$ plane are the preferred method of visualisaion. To capture the continuity of transition between subdomains of distinct diffusivity, the contour levels must be identical. On the other hand, the range of u inherent to each subdomain is different and gradients are acutely non-linear. Hence the level set was taken as the union of adequate values within the range of u restricted to the relevant sector of the spherical shell. The exact choice of levels was compelled by a reasonable depiction of the qualitative terrain in each case, and albeit non-trivial, it was not instructive and thus omitted. Respective tridimensional interactive spherical projections are provided in the supplementary material as figures saved in MATLAB `*.fig` [25] and Octave `*.ofig` [11] (free source) formats, and can be opened using the built-in function `hgload` in the command line or by double-clicking if using the applications' interface. The following quantities evince no qualitative impact on the flow field: $r_{\mathcal{C}}$, $r_{\mathcal{X}}$, $u_{\mathcal{C}}$, $u_{\mathcal{X}}$, γ and C. The choices $r_{\mathcal{X}} = 1$ and $u_{\mathcal{X}} = 1$ can be made without loss of generality by an appropriate non-dimensionalisation. The angle

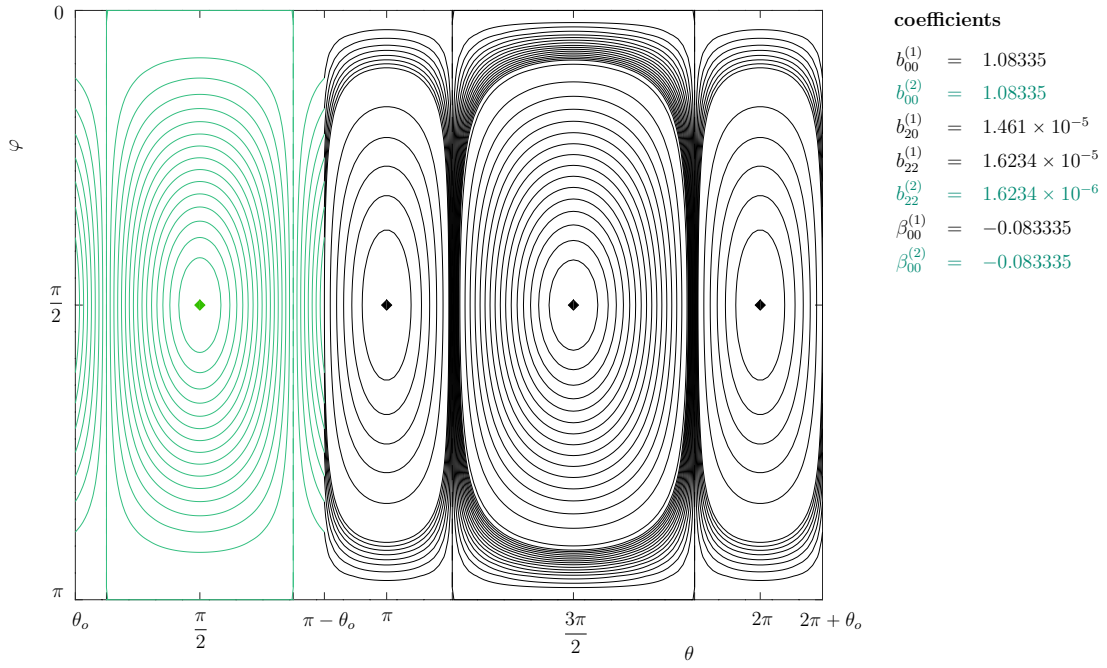

Figure 3: Flow field $u\Big((r_{\mathcal{C}} + r_{\mathcal{X}})/2, \varphi, \theta\Big)$ with $n \leqslant 2$. Green / grey: $\theta_o \leqslant \theta \leqslant \pi - \theta_o$, $K_2 = 10^{-6}$; black: $\pi - \theta_o \leqslant \theta \leqslant 2\pi + \theta_o$, $K_1 = 10^{-7}$. Input parameters: $r_{\mathcal{C}} = 0.1$, $r_{\mathcal{X}} = 1$, $u_{\mathcal{C}} = 0.5$, $u_{\mathcal{X}} = 1$, $\theta_o = \pi/6$, $\gamma = 2$, $C = 5 \times 10^{-12}$. All coefficients equal 0 except as stated. Diamonds mark fixed points. Pole-to-pole separatrices coincide with contour lines, θ coordinates thereof given by equation (14).

θ_o and diffusivities K_i strongly affect the existence and location of topological features such as separatrices and fixed points. These are explored in §3.2. Furthermore, the contour shape is extremely sensitive to the optional parameters – all free coefficients besides the pair determined via boundary conditions.

Figure 3 depicts the basic flow field with all optional parameters set to zero. Note the smoothness of all contours within the respective subdomains and the continuous, yet non-smooth transition on the contiguity planes, entailing an abrupt gradient as evidenced by an increase in contour density. Observe that similar gradients are induced in the proximity of the two pole-to-pole separatrices within the larger (black) sector. This attests to the global impact a jump in diffusivity might engender. Integration of the velocity field with the purpose of obtaining streamlines is stiff, and the sensitivity of the location of these secondary (away from the contiguity interfaces) gradients to problem parameters puts it beyond the ambit of the current study.

The disparity in magnitude of coefficients determined by boundary conditions, as compared to those ensuing by continuity requirements, confirms the dominance of the former. Both poles are, as expected, fixed points, and in this example their type is a saddle, as is seen from the shape of the contours near $\varphi = 0$ and $\varphi = \pi$. It is explicit in the tridimensional spherical projection given in the supplementary file `figure3_3Dproj`. In addition there are four fixed points of the node type: one in the smaller sector (green / grey) and three in the bigger one (black). The respective basins are separated by pole-to-pole separatrices, each lying on a great circle. This basic flow pattern is sensitive to variation in the optional coefficients. For instance, the topological features change dramatically upon a slight adjustment of the degree of freedom $b_{20}^{(2)} : 0 \longmapsto -10^{-4}$ (figure 4). Now there are two nodes, both in the bigger sector; two saddles, one in each sector; and two "figure eight" separatrices that do not pass through either pole. One of these extends over the entire range of θ, whereas the other spans only a part thereof. Furthermore, the shape of the top and bottom isocontours indicates both poles morphed into node points (see also the tridimensional depiction in the supplementary file `figure4_3Dproj`). Yet another adjustment $\beta_{20}^{(i)} : 0 \longmapsto 10^{-5}$ turns the saddle in the smaller sector into a node and reorders the fixed points in the bigger sector from a sequence of node-saddle-node into saddle-node-saddle. The two separatrices become a single "figure eight" contour,

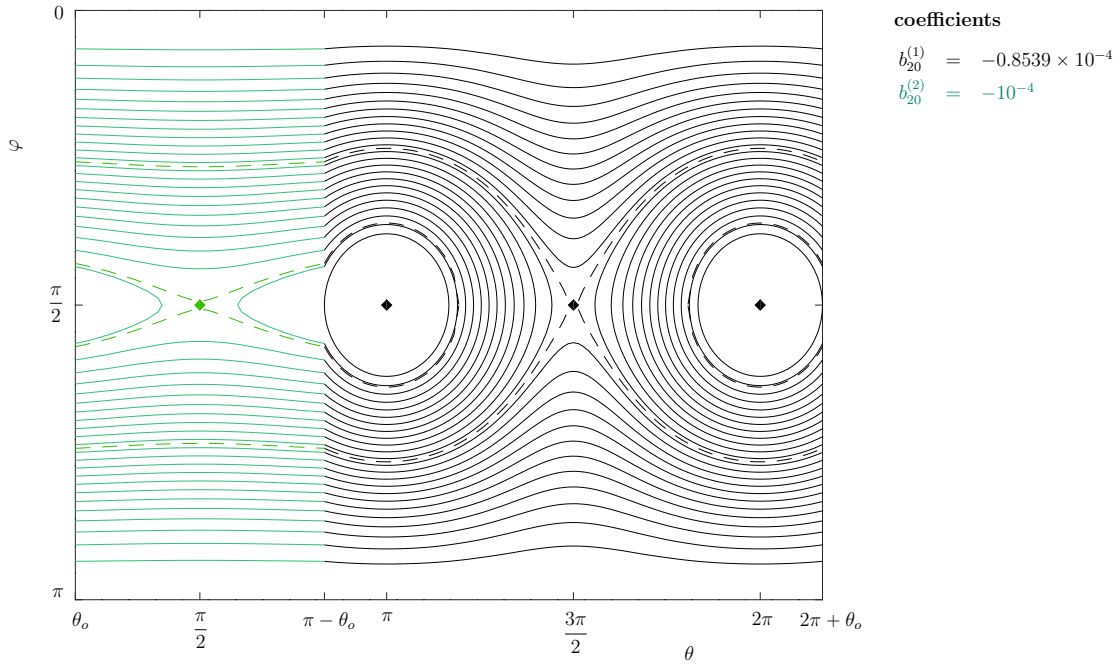

Figure 4: Flow field $u\Big((r_{\mathcal{C}}+r_{\mathcal{X}})/2, \varphi, \theta\Big)$. Configuration, colour scheme, input parameters and all coefficients as in figure 3 except as stated. Diamonds mark fixed points, dashed curves mark separatrices.

but with two crossing points (figure 5 and supplementary files `figure5_3Dproj`). This response to a small variation of the unconstrained coefficients attests to the strong non-linearity of the flow pattern and is formally analysed in §3.2.

3.2 Topological features for $n \leqslant 2$

The fixed points visible in the sample flow patterns in figures 3–5 do not in reality constitute formal stagnation points of the tridimensional flow field, since the gradient of u vanishes only in the two angular directions, but not in the radial one. Intriguingly the qualitative topology of the pattern restricted to a spherical shell of a given radius r is independent of r. From the vantage point of physics, one could trace the locus of each fixed point in space from the core shell $r = r_{\mathcal{C}}$ to the external one $r = r_{\mathcal{X}}$ by a path, whose curvature is expected to be small. At any point along this path a particle is subject to a purely radial motion.

As was shown above, the configuration with $\theta_o = 0$ allowed for more degrees of freedom in the choice of coefficients than $\theta_o \neq 0$. To analyse the more prominent topological features, the attention is limited to a solution u that is valid for any $-\pi/2 < \theta_o < \pi/2$, $\theta_o \neq \pm\pi/4$:

$$u_i^{\gamma} = -\frac{\gamma C}{6K_i}\, r^2 + b_{00} + \frac{\beta_{00}}{r} + \cos\varphi\left(r b_{10} + \frac{\beta_{10}}{r^2}\right) + \frac{3}{2}\left(\frac{1}{2}\cos(2\varphi) + \frac{1}{6}\right)\left(r^2 b_{20}^{(i)} + \frac{\beta_{20}}{r^3}\right) + \frac{3}{2}\Big(1 - \cos(2\varphi)\Big) r^2 b_{22}^{(i)} \cos(2\theta), \tag{12}$$

where equal coefficients in both sectors had the superscript (i) omitted. Differentiating with respect to θ and equating to zero gives

$$\Big(1 - \cos(2\varphi)\Big)\sin(2\theta) = 0. \tag{13a}$$

Thus the points $\varphi = \pi\ell$ and $\theta = \pi\ell/2$, $\ell \in \mathbb{Z}$, form the candidate fixed point set. The points $\varphi = 0, \pi$ correspond to the poles and are roots of $\partial_\varphi u = 0$ as well, establishing the poles are fixed points as expected. When they are excluded from the set of roots of $\partial_\varphi u = 0$, one gets

$$\cos\varphi\left\{2 b_{22}^{(i)} r^2 \cos(2\theta) - \left(r^2 b_{20}^{(i)} + \frac{\beta_{20}}{r^3}\right)\right\} = \frac{1}{3}\left(r b_{10} + \frac{\beta_{10}}{r^2}\right). \tag{13b}$$

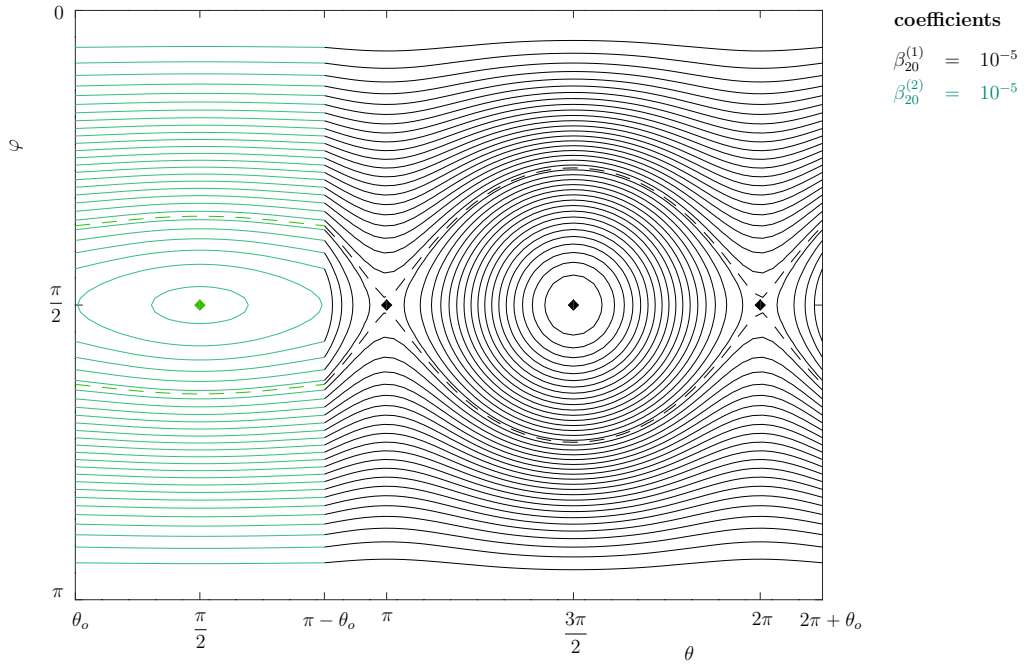

Figure 5: Flow field $u\Big((r_{\mathcal{C}}+r_{\mathcal{X}})/2, \varphi, \theta\Big)$. Configuration, colour scheme, input parameters and all coefficients as in figure 4 except as stated. Diamonds mark fixed points, dashed curves mark separatrices.

If $b_{10} = \beta_{10} = 0$, as is the case in the patterns depicted in figures 3–5, it follows that $\varphi = \pi/2$ or θ must satisfy

$$\cos(2\theta) = \left(r^2 b_{20}^{(i)} + \frac{\beta_{20}}{r^3}\right) \Big/ \left(2b_{22}^{(i)} r^2\right). \tag{14}$$

If the right-hand side in equation (14) is less than unity in magnitude, pole-to-pole loci of fixed points ensue, as in figure 3. By contrast, for the patterns in figures 4 and 5 the right-hand side in (14) exceeds unity, leaving only isolated fixed points on the equator. If at least one of the coefficients b_{10} or β_{10} does not vanish, the fixed points are always located at $\theta = \pi\ell/2$ with φ given by equation (13b), provided the resulting expression for $\cos\varphi$ does not exceed unity in magnitude. One such example with the fixed points off the equator is shown in figure 6 and supplementary file `figure6_3Dproj`.

The separatrix contours are obtained by letting the right-hand side of (12) equal a constant and scrutinising the resulting expression. One observation is that if the coefficient of $\cos(2\varphi)$ vanishes, condition (13b) is recovered. Depending on the other coefficients, either a simple trigonometric equation for φ ensues, giving a set of fixed points as in figures 4 and 5, or the equation is satisfied for all φ, entailing pole-to-pole separatrices as in figure 3. If the term $\cos(2\varphi)$ is retained, the contour might be written as $\tilde{A}_1(r)\Big(\cos\varphi - \tilde{B}_1(r)\Big)^2 + \tilde{A}_2(r,\theta)\sin^2\varphi = 1$ with functions $\tilde{A}_1$, $\tilde{A}_2$ and $\tilde{B}_1$ following by rearrangement of equation (12) into this form, and thus viewed as a generalised ellipse. This is a quadratic equation in $\cos\varphi$ with coefficients depending on $\cos(2\theta)$. This defines a contour $\varphi(\theta)$ that is closed in the plane $\theta - \varphi$, provided that the discriminant gives a real solution, and that the eventual solution for $\cos\varphi$ does not exceed unity in magnitude. The dashed trajectories in figures 4 and 5 were computed thereby. Indeed every isocline in these figures satisfies this equation. One might distinguish between two types of contours: trajectories that span the full range $0 \leqslant \theta \leqslant 2\pi$, and those that do not. The former must perforce traverse both sectors, whilst the latter might or might not be confined to a single sector. Figure 5 contains examples of all three cases. One of the more remarkable characteristics is the disparity in the range of φ and θ that a single isocline might span. A contour might traverse most of the range in *both* φ and θ: for instance, tracing the curve above the green / grey closed contours in figure 6 from left to right begets a latitude variation of about $\pi/4$; this curve then continues into the second sector, skirts the bottom of the first set of closed black contours, ascends

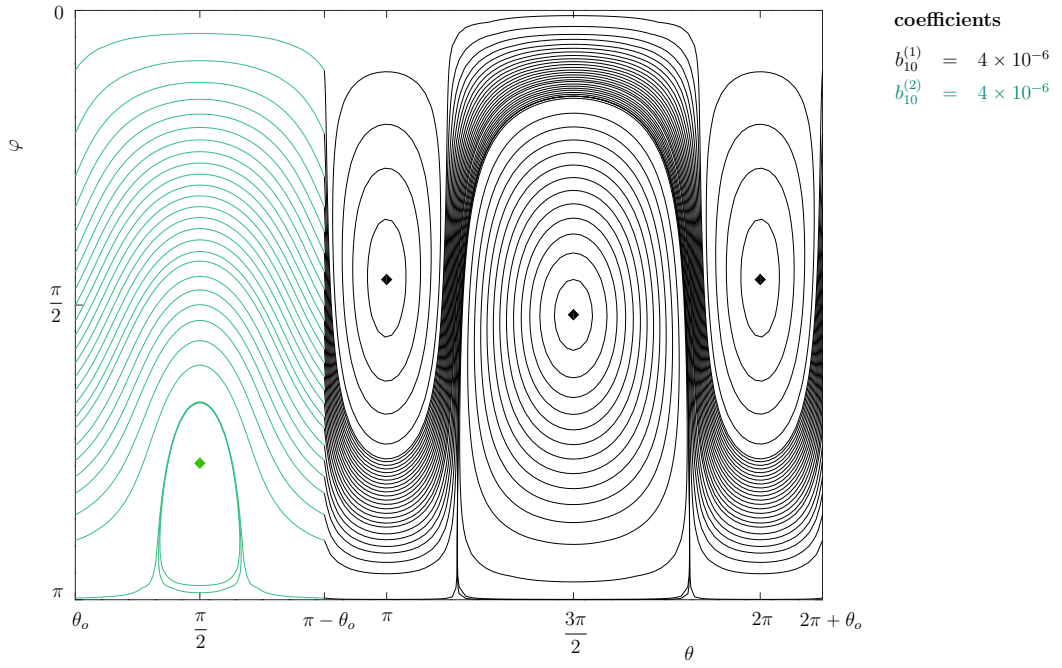

Figure 6: Flow field $u\Big((r_{\mathcal{C}}+r_{\mathcal{X}})/2, \varphi, \theta\Big)$. Configuration, colour scheme, input parameters and all coefficients as in figure 3 except as stated. Diamonds mark fixed points, φ coordinates given by equation (13b).

into the northern hemisphere as it circumnavigates the second fixed point and returns to the vicinity of the south pole. By contrast, a contour might be a local closed trajectory, such as the lowermost contour in the green / grey sector, or any of the smaller closed contours around the three fixed points in the black sector.

Another intriguing observation concerns the vicinity of the south pole. The green / grey closed contours in figure 6 come very close to touching the line $\varphi = \pi$. The ostensibly open adjacent contour is in fact closed, as both its ends do touch $\varphi = \pi$ with different values of θ. This means that although the south pole is a saddle point, it is a peculiar one with two separatrices merged into a closed contour. In the supplementary tridimensional spherical projection corresponding to figure 6 use the rotation feature to view the neighbourhood of the south pole.

3.3 Flow patterns for $n \geqslant 3$

Harmonics with $n \geqslant 3$ contribute terms independent of any combination of sine, cosine or r powers present in (5). In particular there is no interference with the inhomogeneous term stemming from fluid generation within the domain. Therefore decomposing the associated Legendre functions $\mathcal{P}_n^m$ into elementary functions is no longer necessary. Applying (4) to terms of the form $r^n\mathcal{P}_{n0}$ and $r^{-(n+1)}\mathcal{P}_{n0}$ allows to conclude that $b_{n0}^{(i)}$ and $\beta_{n0}^{(i)}$ must equal in both sectors, and define $b_{n0} := b_{n0}^{(i)}$ and $\beta_{n0} := \beta_{n0}^{(i)}$, $i = \{1, 2\}$. For $m \neq 0$ implementing (4) on planes $\theta = \theta_o$ and $\theta = \pi - \theta_o$ gives

$$\sin\big(m\theta_o\big)\Big(a_{nm}^{(1)} - a_{nm}^{(2)}\Big) = 0, \qquad \cos\big(m\theta_o\big)\Big(b_{nm}^{(1)} - b_{nm}^{(2)}\Big) = 0, \tag{15a}$$

$$\cos\big(m\theta_o\big)\Big(K_1 a_{nm}^{(1)} - K_2 a_{nm}^{(2)}\Big) = 0, \qquad \sin\big(m\theta_o\big)\Big(K_1 b_{nm}^{(1)} - K_2 b_{nm}^{(2)}\Big) = 0. \tag{15b}$$

Thus if $\sin\big(m\theta_o\big) \neq 0$ and $\cos\big(m\theta_o\big) \neq 0$, the only possible solution is the trivial one. If $\theta_o = \pi\ell/m$ for some apposite integer ℓ, the first equality in (15a) and the second one in (15b) are satisfied automatically. Then $b_{nm} := b_{nm}^{(i)}$ and $a_{nm}^{(2)} = K_1 \Big/ K_2\, a_{nm}^{(1)}$. If $\theta_o = \pi/(2m) + \pi\ell/m$, similarly $a_{nm} := a_{nm}^{(i)}$ and $b_{nm}^{(2)} = K_1 \Big/ K_2\, b_{nm}^{(1)}$. Swapping $a_{nm}^{(i)} \longleftrightarrow \alpha_{nm}^{(i)}$ and $b_{nm}^{(i)} \longleftrightarrow \beta_{nm}^{(i)}$ will give the respective results for those coefficients. In particular

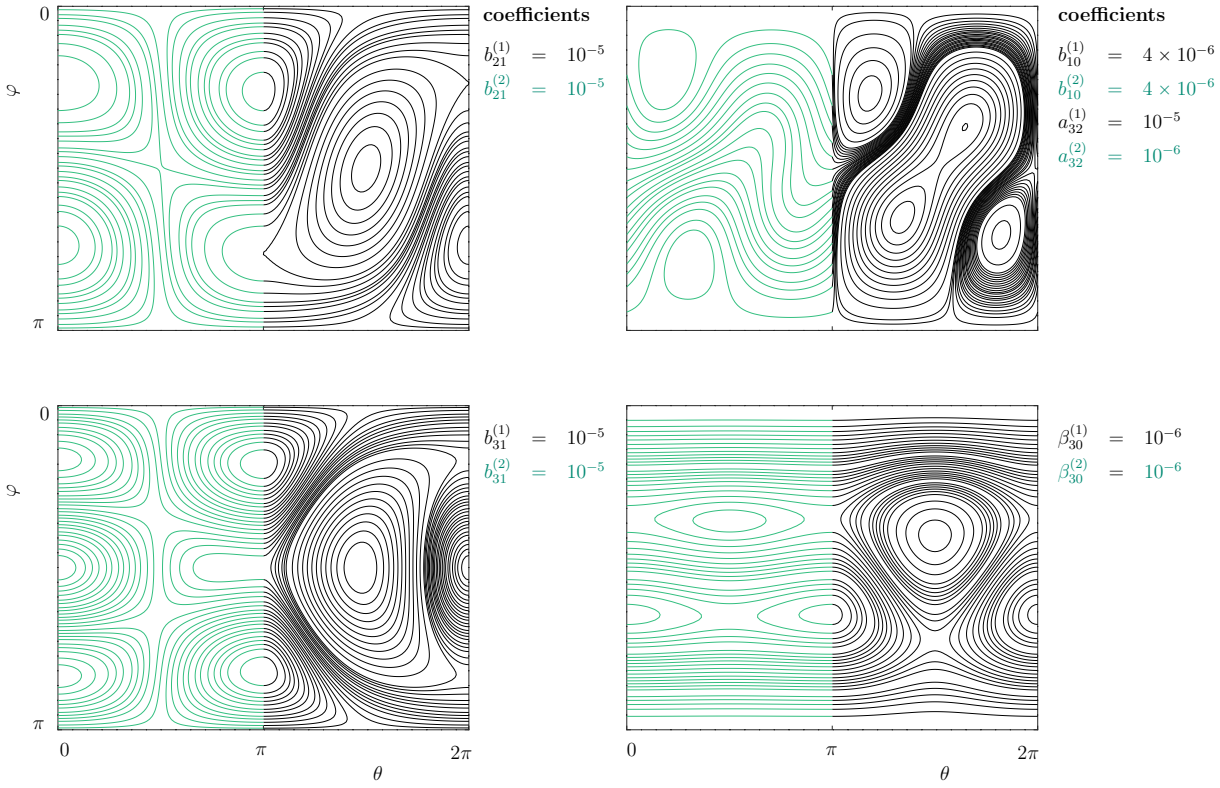

Figure 7: Flow field $u\Big((r_{\mathcal{C}} + r_{\mathcal{X}})/2, \varphi, \theta\Big)$. $\theta_o = 0$. Colour scheme, input parameters and all coefficients as in figure 3 except $b_{22}^{(1)} = 8.1168 \times 10^{-6}$, $b_{22}^{(2)} = 8.1168 \times 10^{-7}$ and values stated by each panel.

the angles that will allow additional degrees of freedom for $m = 3$ are $\theta_o = 0, \pm\pi/6, \pm\pi/3$. Some combinations of m and ℓ result in $\theta_o = \pm\pi/4$. These angles were shown to be singular in the course of the analysis with $n \leqslant 2$ and must be excluded here as well. Note that all angles resulting from solving $\sin(m\theta_o) = 0$ or $\cos(m\theta_o) = 0$ accord two degrees of freedom within any quadruple $\left\{a_{nm}^{(i)}, b_{nm}^{(i)}\right\}$, $i = \{1, 2\}$. Scrutiny of system (15) suggests that a codimension of 2 is the only one possible: a root of $\sin(m\theta_o)$ or $\cos(m\theta_o)$ always removes exactly two equations, as the sine and cosine functions have no common roots. This codimension is directly expressed via a matrix rank for any number of sectors $N \geqslant 2$ in §4. For $N = 3$ and $N = 4$ the codimension equals unity [27]. Figure 7 gives examples of the variety of asymmetric flow patterns conduced by these additional degrees of freedom. Note the appearance of multiple saddle-node mixed points: on the top left panel the upper one out of the pair at $\theta = 0$ and the lower one at $\theta = \pi$; on the bottom left panel the lower and upper ones out of the triple at $\theta = 0$ and the middle one at $\theta = \pi$. A companion graphical user interface allows for further exploration of these flow patterns [3].

4 An arbitrary number of sectors

Implementing equations (4) for a configuration of N sectors leads to a system of linear equations of size $2N \times 2N$ involving an (almost) block bidiagonal matrix:

$$\mathrm{C}^{(m)}\mathbf{c} = \mathbf{r}, \tag{16a}$$

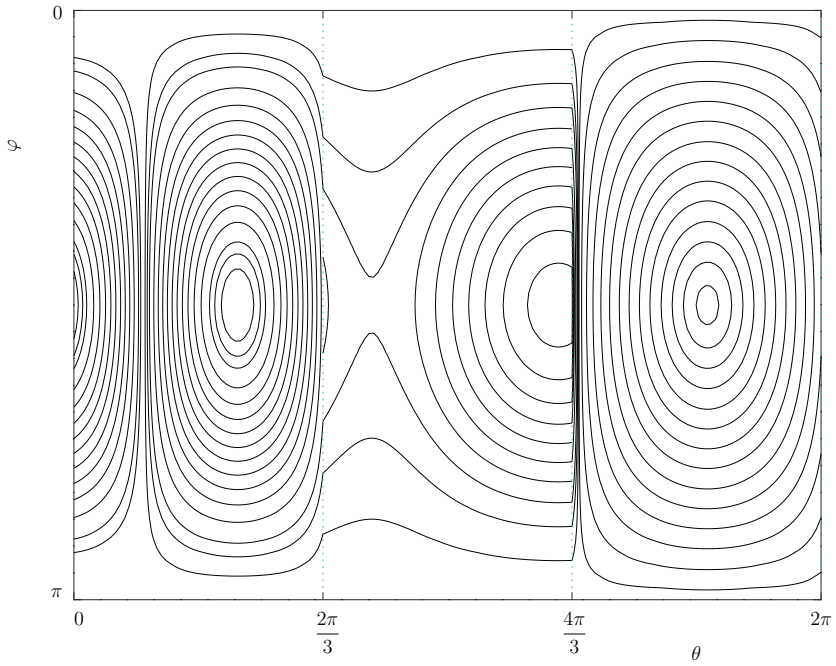

coefficients

$b_{00}^{(1)} = 66735$
$b_{00}^{(2)} = 667350$
$b_{00}^{(3)} = 6673.5$
$b_{20}^{(2)} = -9$
$b_{20}^{(3)} = 0.9$
$b_{22}^{(1)} = -1.8404$
$b_{22}^{(2)} = -0.78723$
$b_{22}^{(3)} = 0.26596$
$a_{22}^{(1)} = a_{22}^{(3)} = 0.75547$
$a_{22}^{(2)} = 2.5797$
$\beta_{00}^{(1)} = -5133.5$
$\beta_{00}^{(2)} = -51335$
$\beta_{00}^{(3)} = -513.35$

Figure 8: Flow field $u\Big((r_{\mathcal{C}} + r_{\mathcal{X}})/2, \varphi, \theta\Big)$. Sector angles $\theta_i = \Big\{\frac{2\pi}{3}, \frac{4\pi}{3}, 2\pi\Big\}$. Respective diffusivities: $K_i = \Big\{10^{-7}, 10^{-6}, 10^{-8}\Big\}$. Input parameters as in figure 3. All coefficients equal 0 except as stated.

$$\mathrm{C}^{(m)} = \begin{pmatrix} \mathrm{A}_1^{(m)} & \mathrm{B}_1^{(m)} & & & \\ & \mathrm{A}_2^{(m)} & \mathrm{B}_2^{(m)} & & \\ & & \ddots & \ddots & \\ & & & \mathrm{A}_{N-1}^{(m)} & \mathrm{B}_{N-1}^{(m)} \\ \mathrm{B}_N^{(m)} & & & & \mathrm{A}_N^{(m)} \end{pmatrix} \tag{16b}$$

with the block matrices given by

$$\mathrm{A}_i^{(m)} = \begin{pmatrix} \sin(m\theta_i) & \cos(m\theta_i) \\ \cos(m\theta_i) & -\sin(m\theta_i) \end{pmatrix}, \qquad \mathrm{B}_i^{(m)} = \begin{pmatrix} -k_i \sin(m\theta_i) & -k_i \cos(m\theta_i) \\ -\cos(m\theta_i) & \sin(m\theta_i) \end{pmatrix}. \tag{16c}$$

For each harmonic (m, n) the unknown vector $\mathbf{c}$ consists of the coefficients in (3a) arranged in pairs in the order of the sectors: $\mathbf{c}_{mn} = \Big(a_{mn}^{(1)},\ b_{mn}^{(1)},\ \cdots,\ a_{mn}^{(N)},\ b_{mn}^{(N)}\Big)^{\mathrm{T}}$ or $\boldsymbol{\gamma}_{mn} = \Big(\alpha_{mn}^{(1)},\ \beta_{mn}^{(1)},\ \cdots,\ \alpha_{mn}^{(N)},\ \beta_{mn}^{(N)}\Big)^{\mathrm{T}}$. The system is inhomogeneous for $m = 2$ and homogeneous for all other harmonics m regardless of the value of n. Interestingly, a matrix of this type appears in the analysis of a particular case of equation (1) with $\gamma = 2$ in polar coordinates, cf. [27, equation (7c)]. In that problem the manifold defined by $\det \mathrm{C}^{(2)} = 0$ is singular, prohibiting the existence of a steady state solution of the separation of variables kind, or depending on the boundary conditions, any steady state at all. Here a similar structure emerges as part of a more convoluted mosaic of arguments, where one must reconcile conditions pertaining to different groups of coefficients. Complete technical detail is provided in appendix A.

Figure 8 depicts the flow pattern for a configuration of three equal sectors with the maximal number of coefficients set to zero. Both poles are fixed points of a mixed type: in the sector $2\pi/3 \leqslant \theta \leqslant 4\pi/3$ the top and bottom trajectories are characteristic of the node, whereas in the other two sectors they correspond to a saddle. This is better evident in the supplementary spherical projection `figure8_3Dproj`. Configurations with additional degrees of freedom are treated as part of the analysis of the manifolds $\det \mathrm{C}^{(m)} = 0$ in §4.1.

A sufficient condition for the existence of a steady state solution to equation (1) in a configuration comprising N sectors is $\det \mathrm{C}^{(2)} \neq 0$. The solution might be endowed with additional degrees of freedom if $\det \mathrm{C}^{(2)} = 0$ and the right-hand side vector $\mathbf{r}$ is in the column space of $\mathrm{C}^{(2)}$. Since for $N > 2$ this vector

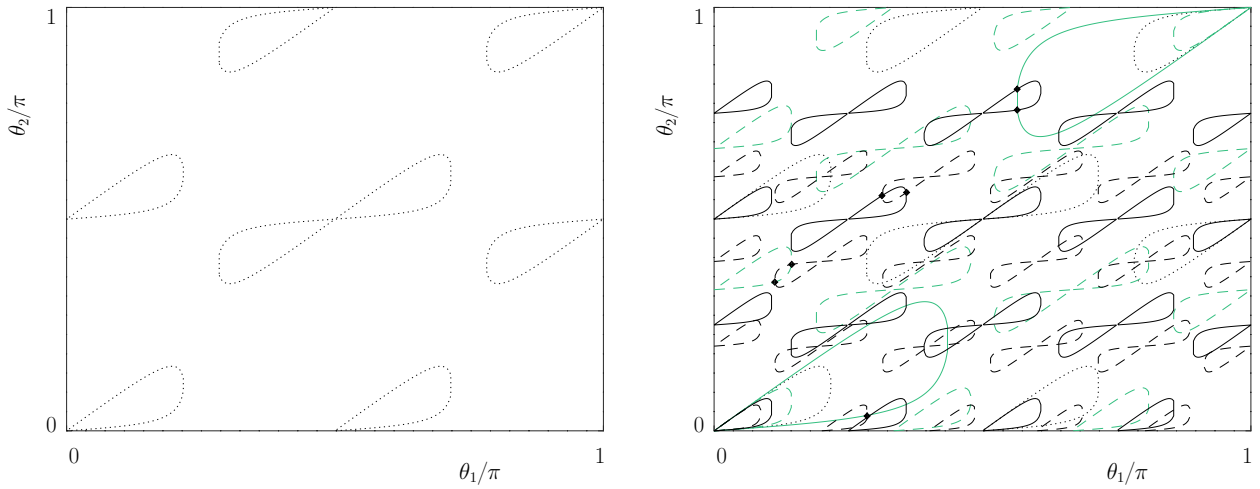

Figure 9: Singular manifold $\det \mathrm{C}^{(2)} = 0$ for a generic three sector configuration $\left\{\theta_1, \theta_2, 2\pi\right\}$ with diffusivities $K_i = \left\{10^{-7}, 10^{-6}, 10^{-8}\right\}$ (dotted black curves, left and right panels). Right panel: superimposed manifolds $\det \mathrm{C}^{(1)} = 0$ (solid green / grey), $\det \mathrm{C}^{(3)} = 0$ (dashed green / grey), $\det \mathrm{C}^{(4)} = 0$ (solid black), $\det \mathrm{C}^{(5)} = 0$ (dashed black). Diamonds mark example intersection points.

depends only on diffusivity ratios, whilst the entries of $\mathrm{C}^{(2)}$ depend both thereon and θ_i, the likelihood of this happening in practice is small. The shape of the singular manifold $\det \mathrm{C}^{(2)} = 0$ was delineated in [27] and its interrelation with $\det \mathrm{C}^{(m)} = 0$ for $m \neq 2$ is further discussed in §4.1. For the solution to allow harmonics with $m \neq 2$ the condition $\det \mathrm{C}^{(m)} = 0$ must hold. The number of degrees of freedom within any one vector $\mathbf{c}_{nm}$ or $\boldsymbol{\gamma}_{nm}$ equals $2N - \operatorname{rank} \mathrm{C}^{(m)}$. For $N = 2$ examples with this codimension equal to 2 were constructed above, in keeping with the degeneracy of the manifold $\det \mathrm{C}^{(m)} = 0$ in that configuration established in [27]. Therein it is further proved that for $N = 3$ and $N = 4$ the codimension cannot exceed unity and conjectured no degeneracy is to appear for a larger number of sectors.

4.1 Manifolds $\det \mathrm{C}^{(m)} = 0$ and degrees of freedom

Rigorous results on the structure and properties of the manifold $\det \mathrm{C}^{(2)} = 0$ were derived in [27]. Here use will be made of its explicit form. For two sectors the manifold is entirely free of dependence on diffusivities [27, equation (10)]:

$$\cos\big(4(\theta_2 - \theta_1)\big) = 1 \tag{17}$$

and can be reduced to the line $\theta_2 - \theta_1 = \pi/2$. Hence as long as the sectors are not right-angled, a steady state solution exists. To open the possibility of additional degrees of freedom for a frequency $m \neq 2$, one must have $\det \mathrm{C}^{(m)} = 0$ whilst $\det \mathrm{C}^{(2)} \neq 0$. To generalise (17) for any m observe that it originated from the matrix $\mathrm{C}^{(2)}$, whose entries contained sines and cosines of the angles $2\theta_i$, and no other dependence on θ_i. Since the matrix $\mathrm{C}^{(m)}$ contains the same entries, but of angles $m\theta_i$, the mapping $\theta_i \longmapsto m\theta_i/2$ gives the required manifold as $\theta_2 - \theta_1 = \pi\ell/m$, where ℓ is an apposite integer. For instance with $m = 1$ and $\ell = 1$ one gets $\theta_2 - \theta_1 = \pi$, i.e. equal sectors. Without loss of generality this corresponds to $\theta_o = 0$, an angle that emerged multiple times in the explicit analysis of the degrees of freedom for $n \leqslant 2$ and $n \geqslant 3$ harmonics. For $m = 3$ the relevant options are $\theta_2 - \theta_1 = \pi/3, 2\pi/3$, conforming to $\theta_o = \pm\pi/6, \pm\pi/3$. The respective degrees of freedom accorded by these configurations were discussed as part of the solution to system (15).

For three sectors, upon the foregoing mapping, the manifold $\det \mathrm{C}^{(m)} = 0$ becomes [27, equation (15a)]

$$\begin{aligned}\cos(2m\theta_1)\Big\{\tilde{k}_{12} + \tilde{k}_{13} - \tilde{k}_{23} - 2\Big\} + \cos(2m\theta_2)\Big\{ - \tilde{k}_{12} + \tilde{k}_{13} + \tilde{k}_{23} - 2\Big\} + \\ \cos\big(2m(\theta_2 - \theta_1)\big)\Big\{\tilde{k}_{12} - \tilde{k}_{13} + \tilde{k}_{23} - 2\Big\} = \tilde{k}_{12} + \tilde{k}_{13} + \tilde{k}_{23} - 6,\end{aligned} \tag{18}$$

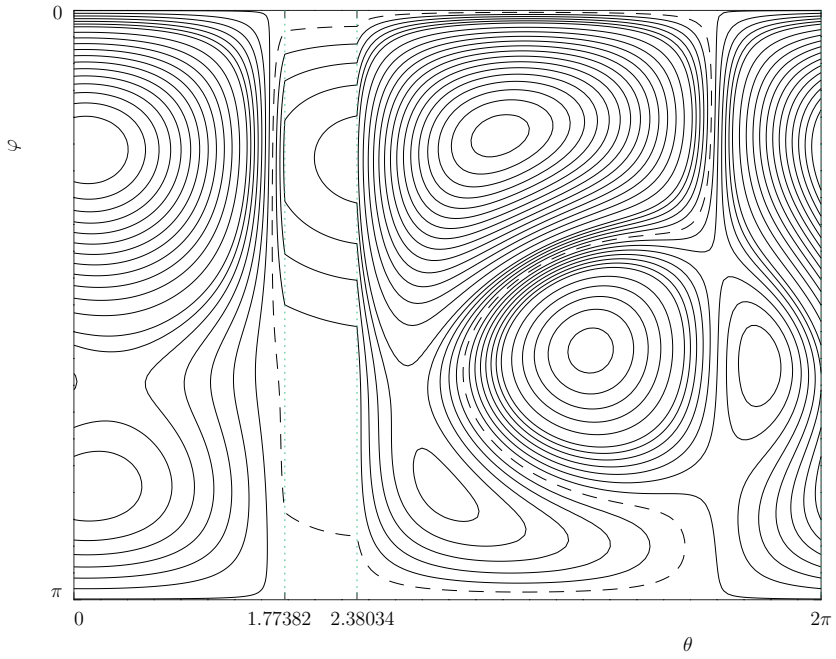

coefficients

$b_{00}^{(i)}$	as in figure 8	
$b_{20}^{(i)}$	as in figure 8	
$b_{n1}^{(1)}$	=	$12.15,\ 1 \leqslant n \leqslant 3$
$b_{n1}^{(2)}$	=	$14.818,\ 1 \leqslant n \leqslant 3$
$b_{n1}^{(3)}$	=	$1.215,\ 1 \leqslant n \leqslant 3$
$b_{22}^{(1)}$	=	-0.25183
$b_{22}^{(2)}$	=	0.41104
$b_{22}^{(3)}$	=	0.42482
$a_{22}^{(1)}$	=	$a_{22}^{(3)} = -0.47716$
$a_{22}^{(2)}$	=	-0.19216
$a_{n1}^{(1)}$	=	$a_{n1}^{(3)} = 1,\ 1 \leqslant n \leqslant 3$
$a_{n1}^{(2)}$	=	$-11.961,\ 1 \leqslant n \leqslant 3$
$\beta_{00}^{(i)}$	as in figure 8	

Figure 10: Flow field $u\Big((r_{\mathcal{C}} + r_{\mathcal{X}})/2, \varphi, \theta\Big)$. Sector angles $\theta_i = \Big\{1.77382, 2.38034, 2\pi\Big\}$ conform to the lower of the two intersection points of $m = 1$ and $m = 4$ orbits in figure 9. Respective diffusivities: $K_i = \Big\{10^{-7}, 10^{-6}, 10^{-8}\Big\}$. Input parameters as in figure 3. All coefficients equal 0 except as stated.

where $\tilde{k}_{ij} = K_i \Big/ K_j + K_j \Big/ K_i$. The left panel of figure 9 shows a typical shape of this manifold with $m = 2$ for a configuration, where $\theta_3 = 2\pi$ without loss of generality due to the rotational invariance of equation (1). The explicit formula for the petal shaped orbits is found in [27]. For most angles θ_1 drawing a vertical line and limiting the attention to one half of the plane with $\theta_2 > \theta_1$ results in a number of intersections. For these values of θ_2 no steady state solution exists. For some ranges of θ_1 there are no intersections, i.e. any value of θ_2 might be picked. These are referred to as regularity corridors. In the right panel of figure 9 the orbits of the concomitant manifolds with $m = 1$ and $3 \leqslant m \leqslant 5$ are superimposed. This plot should be read as follows. To identify a configuration, where a steady state solution (involving $m = 2$ harmonics) exists and additional degrees of freedom with $m \neq 2$ are allowed, one must find combinations (θ_1, θ_2) that lie on the orbits corresponding to the desired harmonics, but avoiding the dotted contours. For instance, for any θ_1 within one of the regularity corridors all solid and dashed orbits offer configurations according degrees of freedom associated with the respective frequency m. Some of these orbits intersect, so it is possible to have degrees of freedom with $m = 4$ and $m = 5$ simultaneously (solid and dashed black), $m = 1$ and $m = 4$ (solid black and green / grey), $m = 3$ and $m = 5$ (dashed black and green / grey), and many other combinations. All these examples are marked with pairs of black diamonds. Outside of the regularity corridors combinations might be similarly constructed, only care must be taken to avoid the singular dotted orbits.

Figure 10 depicts the flow pattern for an example, where harmonics with $m = 1$ and $m = 4$ are allowed to co-exist. The associated degrees of freedom endow the flow field with an impressive variety of topological terrain. There are three features of note. One, the curved contours in the northern half of the narrow sector $1.77382 \leqslant \theta \leqslant 2.38034$ imply a fixed point of the node type. However, the curvature of the contours immediately across the contiguity plane to the right of $\theta = 2.38034$ renders that part of the saddle type. This shows that a fixed point of a mixed type is also possible in configurations that have no immediately apparent symmetry. The second observation is that the dashed closed contour straddling all three sectors encompasses the aforementioned mixed type point and two more simple node points (as well as one saddle). The same isocline constitutes incoming and outgoing trajectories typical of a saddle point for both poles, but fused into a single closed contour. The third point of interest is that the presence of a narrow sector with a higher diffusivity gives rise to multiple fixed points and a variegated pattern of basins in the other

sectors, to wit the impact of one narrow preferential direction might be global and significant.

A generic combination of two co-existing harmonics is constructed by choosing two desired values of m and creating a system of two equations in two unknowns (θ_1, θ_2) from (18). Some pairs of m values, e.g. $m = 1$ and $m = 3$, result in no intersections. If this system does possess a solution, it is likely not unique, as the orbits are closed – begetting paired solutions – and furthermore replicated periodically. For higher values of N the petal-shaped orbits persist on any planar cross-section of the $(N-1)$-dimensional manifold (with the last contiguity azimuth set to $\theta_N = 2\pi$ and K_i specified), but their orientation, area and proximity to one another vary greatly, cf. [27, figure 7]. Via a similar construction with $N-1$ values of m one might find some N-tuples of θ_i that accord additional degrees of freedom. Furthermore, since $N-1$ more parameters in the form of diffusivity ratios $k_i = K_i \Big/ K_{i+1}$ are available, it might be possible to tune those so that three or more contours intersect at the same point. In figure 9 this is exemplified by the trifold intersection of $m = 1$, $m = 4$ and $m = 5$ orbits marked by a lone (unpaired) diamond. In this particular example $\theta_2 < \theta_1$. Therefore the correct contiguity angle layout must be obtained by adding π to the value of θ_2, as the relevant period is that of the manifold corresponding to the harmonic $m = 1$.

5 Conclusion

The steady non-linear diffusion equation with an azimuthal piecewise constant anisotropy admits a wide class of exact solutions in spherical coordinates. Within each sector the solution is a series comprising tesseral and sectoral harmonics written via the associated Legendre functions of degree n and order m, $m \leqslant n$. The harmonics with $m = n = 2$ are essential if the fluid generation rate within the domain is not zero. The presence of other combinations of m and n is governed by a set of manifolds defined via the determinant of the matrix $\mathrm{C}^{(m)}$. Solution existence is guaranteed if $\det \mathrm{C}^{(2)} \neq 0$. By contrast, for a degree of freedom associated with harmonic $m \neq 2$ (and any value of n) to be present, $\det \mathrm{C}^{(m)}$ must vanish. The constraint $\det \mathrm{C}^{(2)} \neq 0$ as a sufficient condition for the solution existence first emerged in the context of exact solutions in the simpler framework of a planar flow in polar coordinates [27]. The question whether the topology of this singular manifold is an inherent structure of the non-linear diffusion equation *regardless* of dimension and system of coordinates, is a topic of future study.

Due to the abrupt change of diffusivity between adjacent subdomains the contours of u are not smooth on the contiguity surfaces. This phenomenon has been observed in experimental studies of a plume traversing a sharp interface between two distinct porous media [31], but has not been hitherto modelled mathematically with multiple interfaces. The anisotropy also gives rise to a new type of fixed point that is neither a node nor a saddle, but commingles the local terrain attributes of both. Such points are located on contiguity planes between sectors, with each sector responsible for a part of the contour that would have been a pure node or saddle, had the solution therein been extended to the entire range of the azimuthal angle θ. When sectors contribute contours of distinct types, the result is a fixed point of a mixed type. Moreover, when such point is located at the pole, any permutation of an N-tuple of saddle and node contributions is possible. This topological feature is new and cannot be obtained without the presence of anisotropy.

The inherent abundance of fixed points associated with $u(r, \varphi, \theta)$ restricted to a shell of radius r and the striking variability of their basins of attraction or repulsion, conduce one fundamental inference: when the radial symmetry is broken by anisotropy, radial transport becomes surprisingly ineffective. The only dependence of u^γ on r is of the power law type. Therefore all three components of ∇u are proportional to the same power of r: the radial velocity by differentiation, and the polar and azimuthal velocity via the factor $1/r$. Any generic boundary condition is bound to invoke all harmonics, including those with negative powers of r. The dimensionless outer radius is $r_{\mathcal{X}} = 1$ and the core radius satisfies $r_{\mathcal{C}} \ll 1$. Thus as $r \longrightarrow r_{\mathcal{C}}^+$, all three velocity components become large. If the highest harmonic present is n, the magnitude of u itself and its gradient are $u \sim \mathcal{O}\Big(r^{-(n+1)/\gamma}\Big)$ and $\nabla u \sim \mathcal{O}\Big(r^{-1-(n+1)/\gamma}\Big)$ respectively. Since all gradient components are of the same magnitude, a fraction as large as $2/3$ of the diffusant's kinetic energy – proportional to $|\nabla u|^2$ – is associated with motion tangential to the spherical shell. In wells, whose purpose is to collect fluid, this translates to an increase of the energy required to maintain a desired radial flowrate and diminution of the zone of influence. The only way to avoid that is to eliminate anisotropy. Narrow wedges of higher or lower diffusivity engender strong tangential flow throughout the domain. Nevertheless, the existence of preferential directions of flow might be crucial for a successful function of a well, whose installation is extremely difficult (for instance, offshore), whilst the reservoir is large [37]. In an application such as aquifer remediation, where

the well's purpose is to inject fluid, the strong polar and azimuthal currents might be beneficial in the sense that the performance of active compounds will improve due to mixing, at the expense of compromised radial reach. In the biomedical example of exploration of the extracellular space of the brain [30], particles are set to perform a random walk for the purpose of revealing an unknown terrain of obstacles. The anisotropy will enhance walk pattern variety and thus identify the space structure with fewer walkers.

In summary, the introduction of anisotropy breaks the spherical radial symmetry and profoundly impacts the flow pattern, entailing strong polar and azimuthal velocities, whose magnitude is comparable with that of the radial motion. The existence of a narrow sector of a distinct diffusivity suffices to create a tessellation of attraction and repulsion basins in the other sectors, greatly diminishing the effectiveness of the radial transport. The quantitative exploration of local and global fluxes as well as flow pattern control via diffusivities is a topic of future study.

Acknowledgement

The financial support and mobility accorded by MITACS Globalink Research Internship programme (Canada) is gratefully acknowledged. The authors thank Prof. Richard Taylor of Thompson Rivers University, British Columbia, Canada, for insightful discussions.

Appendix A. An arbitrary number of sectors: technical detail

A.1 Harmonics $n \leqslant 2$

For an arbitrary number of sectors the derivation is more elegant if (5) is rewritten as

$$\frac{6K_i}{\gamma C}\,u_i^{\gamma} = -r^2 + b_{00}^{(i)} + \frac{\beta_{00}^{(i)}}{r} + \cos\varphi\left\{ r b_{10}^{(i)} + \frac{\beta_{10}^{(i)}}{r^2} \right\} - \sin\varphi\left\{ r\left(a_{11}^{(i)}\sin\theta + b_{11}^{(i)}\cos\theta\right) + \frac{1}{r^2}\left(\alpha_{11}^{(i)}\sin\theta + \beta_{11}^{(i)}\cos\theta\right) \right\} +$$

$$\frac{3}{2}\left(\frac{1}{2}\cos(2\varphi) + \frac{1}{6}\right)\left\{ r^2 b_{20}^{(i)} + \frac{\beta_{20}^{(i)}}{r^3} \right\} - \frac{3}{2}\sin(2\varphi)\left\{ r^2\left(a_{21}^{(i)}\sin\theta + b_{21}^{(i)}\cos\theta\right) + \frac{1}{r^3}\left(\alpha_{21}^{(i)}\sin\theta + \beta_{21}^{(i)}\cos\theta\right) \right\} +$$

$$\frac{3}{2}\Big(1 - \cos(2\varphi)\Big)\left\{ r^2\left(a_{22}^{(i)}\sin(2\theta) + b_{22}^{(i)}\cos(2\theta)\right) + \frac{1}{r^3}\left(\alpha_{22}^{(i)}\sin(2\theta) + \beta_{22}^{(i)}\cos(2\theta)\right) \right\}. \tag{A1}$$

Beginning with the simplest constant term in (A1), define $k_i = K_i \Big/ K_{i+1}$, $1 \leqslant i \leqslant N$ (as before the last index must wrap back to the first sector via $k_N = K_N/K_1$) and apply conditions (4) to get the linear system

$$b_{00}^{(i)} = k_i b_{00}^{(i+1)}, \qquad 1 \leqslant i \leqslant N. \tag{A2a}$$

Herein and below any recurrence or similar relation involving an index that exceeds the range $1 \leqslant i \leqslant N$, is tacitly mapped $N+1 \longmapsto 1$ or $0 \longmapsto N$ as required for periodicity. Isolating $b_{00}^{(i+1)}$ in terms of $b_{00}^{(i)}$, by mathematical induction it is elementary to arrive at

$$b_{00}^{(i+1)} = b_{00}^{(1)} \Big/ \prod_{\ell=1}^{i} k_\ell. \tag{A2b}$$

To interpret (A2b) for $i = N$, observe that $\prod_{\ell=1}^{N} k_\ell = 1$ and furthermore utilise the contiguity of the N-th and first sectors to infer this relation results in an identity. Thus the linear system defined by (A2a) is of rank $N-1$, entailing one degree of freedom. An identical inference follows for $\beta_{00}^{(i)}$, $b_{10}^{(i)}$ and $\beta_{10}^{(i)}$.

Next consider the coefficients of $r\sin\varphi$. Equations (4) yield a system of $2N$ equations in $2N$ unknown coefficients $\left\{a_{11}^{(i)}, b_{11}^{(i)}\right\}$, $1 \leqslant i \leqslant N$:

$$a_{11}^{(i)}\sin\theta_i + b_{11}^{(i)}\cos\theta_i - k_i\left(a_{11}^{(i+1)}\sin\theta_i + b_{11}^{(i+1)}\cos\theta_i\right) = 0, \tag{A3a}$$

$$a_{11}^{(i)}\cos\theta_i - b_{11}^{(i)}\sin\theta_i - a_{11}^{(i+1)}\cos\theta_i + b_{11}^{(i+1)}\sin\theta_i = 0. \tag{A3b}$$

Equations (A3) might be arranged as an (almost) block bidiagonal linear system:

$$\mathrm{C}^{(1)}\mathbf{c}_{11} = \mathbf{0}, \tag{A4a}$$

where the vector $\mathbf{c}_{mn}$ is $\mathbf{c}_{mn} = \left(a_{mn}^{(1)},\ b_{mn}^{(1)},\ \cdots,\ a_{mn}^{(N)},\ b_{mn}^{(N)}\right)^{\mathrm{T}}$, and the matrix $\mathrm{C}^{(m)}$ is defined as

$$\mathrm{C}^{(m)} = \begin{pmatrix} \mathrm{A}_1^{(m)} & \mathrm{B}_1^{(m)} & & & \\ & \mathrm{A}_2^{(m)} & \mathrm{B}_2^{(m)} & & \\ & & \ddots & \ddots & \\ & & & \mathrm{A}_{N-1}^{(m)} & \mathrm{B}_{N-1}^{(m)} \\ \mathrm{B}_N^{(m)} & & & & \mathrm{A}_N^{(m)} \end{pmatrix}, \tag{A4b}$$

with the block matrices given by

$$\mathrm{A}_i^{(m)} = \begin{pmatrix} \sin(m\theta_i) & \cos(m\theta_i) \\ \cos(m\theta_i) & -\sin(m\theta_i) \end{pmatrix}, \qquad \mathrm{B}_i^{(m)} = \begin{pmatrix} -k_i\sin(m\theta_i) & -k_i\cos(m\theta_i) \\ -\cos(m\theta_i) & \sin(m\theta_i) \end{pmatrix}. \tag{A4c}$$

For the negative powers of r define the vector of coefficients $\boldsymbol{\gamma}_{mn} = \left(\alpha_{mn}^{(1)},\ \beta_{mn}^{(1)},\ \cdots,\ \alpha_{mn}^{(N)},\ \beta_{mn}^{(N)}\right)^{\mathrm{T}}$. Then $\boldsymbol{\gamma}_{11}$ satisfies a system identical to (A4a), as do $\mathbf{c}_{21}$ and $\boldsymbol{\gamma}_{21}$. The homogeneity of equation (A4a) implies that if $\det \mathrm{C}^{(1)} \neq 0$, the only solution is $\mathbf{c}_{11} = \mathbf{c}_{21} = \boldsymbol{\gamma}_{11} = \boldsymbol{\gamma}_{21} = \mathbf{0}$. If $\det \mathrm{C}^{(1)} = 0$, some degrees of freedom are expected.

Equations (4) for the terms of the form r^2 in (A1) give

$$-1 + \frac{1}{4}\,b_{20}^{(i)} + \frac{3}{2}\Big(a_{22}^{(i)}\sin(2\theta_i) + b_{22}^{(i)}\cos(2\theta_i)\Big) = k_i\left\{-1 + \frac{1}{4}\,b_{20}^{(i+1)} + \frac{3}{2}\Big(a_{22}^{(i+1)}\sin(2\theta_i) + b_{22}^{(i+1)}\cos(2\theta_i)\Big)\right\} \tag{A5a}$$

and

$$a_{22}^{(i)}\cos(2\theta_i) - b_{22}^{(i)}\sin(2\theta_i) - a_{22}^{(i+1)}\cos(2\theta_i) + b_{22}^{(i+1)}\sin(2\theta_i) = 0 \tag{A5b}$$

respectively. Condition (4a) applied to the $r^2\cos(2\varphi)$ terms gives

$$\frac{3}{4}\,b_{20}^{(i)} - \frac{3}{2}\Big(a_{22}^{(i)}\sin(2\theta_i) + b_{22}^{(i)}\cos(2\theta_i)\Big) = k_i\left\{\frac{3}{4}\,b_{20}^{(i+1)} - \frac{3}{2}\Big(a_{22}^{(i+1)}\sin(2\theta_i) + b_{22}^{(i+1)}\cos(2\theta_i)\Big)\right\}, \tag{A5c}$$

whilst (4b) results in an equation that matches (A5b). System (A5) comprises $3N$ linear equations in $3N$ unknown coefficients $\left\{b_{20}^{(i)}, a_{22}^{(i)}, b_{22}^{(i)}\right\}_{i=1}^{N}$. It is possible to simplify it somewhat. Summing equations (A5a) and (A5c) gives

$$b_{20}^{(i)} = 1 - k_i + k_i b_{20}^{(i+1)}. \tag{A6a}$$

Induction similar to that employed in (A2) gives

$$b_{20}^{(i+1)} = 1 + \left(b_{20}^{(1)} - 1\right) \Bigg/ \prod_{\ell=1}^{i} k_\ell \tag{A6b}$$

with a single degree of freedom, since relation (A6b) for $i = N$ leads to an identity. Note that setting $b_{20}^{(1)} = 1$ will end up in the symmetry $b_{20}^{(i)} = 1\ \forall\ 1 \leqslant i \leqslant N$. Multiplying (A5a) by $\frac{2}{3}$ and rearranging in conjunction with (A5b) yields

$$\mathrm{C}^{(2)}\mathbf{c}_{22} = \mathbf{r}, \tag{A7a}$$

where $\mathrm{C}^{(2)}$ is defined in (A4b) and $\mathbf{c}_{22}$ immediately below (A4a). This time, however, the system is inhomogeneous with the right-hand side vector given by $\mathbf{r} = \frac{1}{2}\Big(1 - k_1,\ 0,\ \cdots,\ 1 - k_N, 0\Big)^{\mathrm{T}}$, where (A6b) was used

to simplify the terms involving $b_{20}^{(i)}$. A procedure of the same ilk for the triple N-tuple $\left\{\beta_{20}^{(i)}, \alpha_{22}^{(i)}, \beta_{22}^{(i)}\right\}_{i=1}^{N}$ leads to a homogeneous counterpart of (A7a), accompanied by a condition identical to (A2b):

$$\mathrm{C}^{(2)}\boldsymbol{\gamma}_{22} = \mathbf{0}, \qquad \beta_{20}^{(i+1)} = \beta_{20}^{(1)} \Bigg/ \prod_{\ell=1}^{i} k_\ell. \tag{A7b}$$

Since system (A7a) is inhomogeneous, there are two possibilities for (A1) to be a viable solution. One, the matrix $\mathrm{C}^{(2)}$ is non-singular, i.e. $\det \mathrm{C}^{(2)} \neq 0$ holds. Then the resulting set of coefficients $\mathbf{c}_{22}$ is unique and contains some non-vanishing entries, whilst $\boldsymbol{\gamma}_{22} = \mathbf{0}$. Two, $\det \mathrm{C}^{(2)} = 0$, but the right-hand side vector $\mathbf{r}$ is within the column space of $\mathrm{C}^{(2)}$. Then both $\mathbf{c}_{22}$ and $\boldsymbol{\gamma}_{22}$ will contain degrees of freedom.

A.2 Harmonics $n \geqslant 3$

As with the two sector configuration, $n \geqslant 3$ harmonics do not interlace with those corresponding to $n \leqslant 2$. Redefining the constants in (3a) in the spirit of (A1) by shifting the ratio $\gamma C/\big(6K_i\big)$ to the left-hand side, applying conditions (4) to terms of the form $r^n\mathcal{P}_n^m$ with $n \geqslant 3$ and utilising the induction technique outlined for $n \leqslant 2$ results in the following relation for the coefficients $b_{n0}^{(i)}$ and a linear system for $\left\{a_{nm}^{(i)}, b_{nm}^{(i)}\right\}_{i=1}^{N}$ when $m \neq 0$:

$$b_{n0}^{(i+1)} = b_{n0}^{(1)} \Bigg/ \prod_{\ell=1}^{i} k_\ell, \qquad \mathrm{C}^{(m)}\mathbf{c}_{nm} = \mathbf{0}, \tag{A8a}$$

where $\mathrm{C}^{(m)}$ is defined in (A4b) and $\mathbf{c}_{nm}$ immediately below (A4a). Identical steps for the functional shape $r^{-(n+1)}\mathcal{P}_n^m$ yield respectively

$$\beta_{n0}^{(i+1)} = \beta_{n0}^{(1)} \Bigg/ \prod_{\ell=1}^{i} k_\ell, \qquad \mathrm{C}^{(m)}\boldsymbol{\gamma}_{nm} = \mathbf{0}, \tag{A8b}$$

where $\boldsymbol{\gamma}_{nm}$ is defined as beneath (A4c). If $\det \mathrm{C}^{(2)} \neq 0$ in the solution $u_i^{\gamma}\Big|_{n\leqslant 2}$, the only solution to equations (A8) with $m = 2$ is $\mathbf{c}_{n2} = \boldsymbol{\gamma}_{n2} = \mathbf{0}$. The requirement $\det \mathrm{C}^{(m)} = 0$ suffices to retain degrees of freedom for coefficients $\left\{a_{nm}^{(i)}, b_{nm}^{(i)}, \alpha_{nm}^{(i)}, \beta_{nm}^{(i)}\right\}$ with any m.

References

[1] W. F. Ames, *Similarity for nonlinear diffusion equation*, Ind. Eng. Chem. Fundamen., 4(1) (1965), pp. 72–76.

[2] D. Anderson and M. Lisak, *Approximate solutions of some nonlinear diffusion equations*, Phys. Rev. A, 22 (1980), pp. 2761–2768.

[3] P. Awasthi, M. Kumar, and Y. Nec, *Anisotropic diffusion in spherical coordinates: steady state wizard*, TRUSpace: open access digital archive `https://tru.arcabc.ca/islandora/object/tru%3A5928`, 2022.

[4] G. I. Barenblatt, *Scaling, self-similarity and intermediate asymptotics*, Cambridge University Press, 1996.

[5] G. I. Barenblatt, V. M. Entov, and V. M. Ryzhik, *Theory of fluid flow through natural rock*, Kluwer, Dodrecht, 1990.

[6] J. G. Berryman and C. J. Holland, *Asymptotic behaviour of the nonlinear diffusion equation* $n_t = \left(n^{-1}n_x\right)_x$, J. Math. Phys., 23 (1982), p. 1982.

[7] G. Bluman and S. Kumei, *On the remarkable nonlinear diffusion equation* $(\partial/\partial x)[a(u+b)^{-2}(\partial u/\partial x)]-(\partial u/\partial t) = 0$, J. Math. Phys., 21(5) (1980), p. 1019.

[8] C. M. Elliott, M. A. Herrero, J. R. King, and J. R. Ockendon, *The mesa problem: Diffusion patterns for* $u_t = \nabla\cdot(u^m\nabla u)$ *as* $m \to +\infty$, IMA J. Appl. Math., 37 (1986), pp. 147–154.

[9] T. D. Frank and R. Friedrich, *Estimating the nonextensivity of systems from experimental data: a nonlinear diffusion equation approach*, Physica A: Stat. Mech. Appl., 347(1) (2005), pp. 65–76.

[10] L. Germanou, M. T. Ho, Y. Zhang, and L. Wu, *Intrinsic and apparent gas permeability of heterogeneous and anisotropic ultra-tight porous media*, J. Nat. Gas Sci. Eng., 60 (2018), pp. 271–283.

[11] GNU, *Octave, 6.2.0*, `https://www.gnu.org/software/octave/index`, 2021.

[12] I. S. Gradshteyn and I. M. Ryzhik, *Table of integrals, series and products*, 4th edition, edited by Alan Jeffrey, Academic Press, 1980.

[13] J. D. Hyman, S. Karra, N. Makedonska, C. W. Gable, S. L. Painter, and H. S. Viswanathan, *dfnworks: a discrete fracture network framework for modeling subsurface flow and transport*, Comp. Geosci., 84 (2015), pp. 10–19.

[14] W. L. Kath and C. S. Donald, *Waiting-time behavior in a nonlinear diffusion equation*, Stud. Appl. Math., 67 (1982), pp. 79–105.

[15] J. R. King, *Approximate solutions to a nonlinear diffusion equation*, J. Eng. Math., 22 (1988), pp. 53–72.

[16] J. R. King, *Exact results for the nonlinear diffusion equations* $\frac{\partial u}{\partial t} = \frac{\partial}{\partial x}\left(u^{-4/3}\frac{\partial u}{\partial x}\right)$ *and* $\frac{\partial u}{\partial t} = \frac{\partial}{\partial x}\left(u^{-2/3}\frac{\partial u}{\partial x}\right)$, J. Phys. A: Math. Gen., 24 (1991), pp. 5721–5745.

[17] J. R. King, *Some non-self-similar solutions to a nonlinear diffusion equation*, J. Phys. A: Math. Gen, 25 (1992), pp. 4861–4868.

[18] J. H. Knight and J. R. Philip, *Exact solutions in nonlinear diffusion*, J. Eng. Math., 8 (1974), pp. 219–227.

[19] A. A. Kosov and E. I. Semenov, *Exact solutions of the nonlinear diffusion equation*, Siberian Math. J., 60(1) (2019), pp. 93–107.

[20] A. A. Lacey, J. R. Ockendon, and A. B. Tayler, *"Waiting-time" solutions of a nonlinear diffusion equation*, SIAM J. Appl. Math., 42(6) (1982), pp. 1252–1264.

[21] E. W. Larsen and G. C. Pomraning, *Asymptotic analysis of nonlinear Marshak waves*, SIAM J. Appl. Math., 39 (1980), pp. 201–212.

[22] N. E. Leont'ev and E. I. Roshchin, *A model of incompressible-fluid flow with a free surface in a highly porous medium*, Fluid Dyn., 53 (2018), pp. 805–811.

[23] P. D. Lundegard and D. LaBrecque, *Air sparging in a sandy aquifer (Florence,Oregon, U.S.A.): actual and apparent radius of influence*, J. Contam. Hydrol., 19 (1995), pp. 1–27.

[24] R. W. Mair, G. P. Wong, D. Hoffmann, M. D. Hürlimann, S. Patz, L. M. Schwartz, and R. L. Walsworth, *Probing porous media with gas diffusion NMR*, Phys. Rev. Lett., 83 (1999), p. 3324.

[25] MATLAB, *9.10.0*, `https://www.mathworks.com`, 2021.

[26] S. Mauran, L. Rigaud, and O. Coudevylle, *Application of the Carman-Kozeny correlation to a high-porosity and anisotropic consolidated medium: the compressed expanded natural graphite*, Transp. Porous Media, 43 (2001), pp. 355–376.

[27] Y. Nec, *Singularities in weakly compressible flow through a porous medium*, Fluid Dyn. Res., 53 (2021), p. 045507.

[28] Y. Nec and G. Huculak, *Landfill gas flow: collection by horizontal wells*, Transp. Porous Media, 130(3) (2019), pp. 769–797.

[29] Y. Nec and G. Huculak, *Exact solutions to radial flow in a porous medium with variable permeability*, Phys. Fluids, 32 (2020), p. 077108.

[30] C. Nicholson and E. Syková, *Extracellular space structure revealed by diffusion analysis*, Trends Neurosci., 21 (1998), pp. 207–215.

[31] C. K. Sahu and M. R. Flynn, *Filling box flows in porous media*, J. Fluid Mech., 782 (2015), pp. 455–478.

[32] H. Vigneault, R. Lefebvre, and M. Nastev, *Numerical simulation of the radius of influence for landfill gas wells*, Vadose Zone J., 3 (2004), pp. 909–916.

[33] V. A. Volpert, A. A. Nepomnyashchy, and Y. Kanevsky, *Drug diffusion in a swollen polymer*, SIAM J. Appl. Math, 78(1) (2018), pp. 124–144.

[34] G. R. Walter, *Fatal flaws in measuring landfill gas generation rates by empirical well testing*, J. Air Waste Manage. Assoc., 53(4) (2003), pp. 461–468.

[35] A. M. Wazwaz, *Exact solutions to nonlinear diffusion equations obtained by the decomposition method*, Appl. Math. Comput., 123(1) (2001), pp. 109–122.

[36] W. R. Wise and T. G. Townsend, *One-dimensional gas flow models for municipal solid waste landfills: cylindrical and spherical symmetries*, J. Environ. Eng., 137(6) (2011), pp. 514–516.

[37] P. Zhang, Y. Zhang, W. Zhang, and S. Tian, *Numerical simulation of gas production from natural gas hydrate deposits with multi-branch wells: influence of reservoir properties*, Energy, 238(A) (2022), p. 121738.